# SYSTEM IDENTIFICATION WITH PARTICULAR INTEREST ON THE HIGH FREQUENCY RADAR UNDER IONOSPHERIC DISTURBANCES

A THESIS SUBMITTED TO
THE GRADUATE SCHOOL OF NATURAL AND APPLIED SCIENCES
OF
MIDDLE EAST TECHNICAL UNIVERSITY

BY

SÜLEYMAN OLCAY BÜYÜKPAPUŞÇU

IN PARTIAL FULFILLMENT OF THE REQUIREMENTS
FOR
THE DEGREE OF MASTER OF SCIENCE
IN
ELECTRICAL AND ELECTRONICS ENGINEERING

FEBRUARY 2007

Approval of the Graduate School of Natural and Applied Sciences.

Prof. Dr. Canan ÖZGEN
Director

I certify that this thesis satisfies all the requirements as a thesis for the degree of Master of Science.

Prof. Dr. İsmet ERKMEN
Head of Department

This is to certify that we have read this thesis and that in our opinion it is fully adequate, in scope and quality, as a thesis for the degree of Master of Science.

Prof. Dr. Yurdanur TULUNAY
Co-Supervisor

Prof. Dr. Ersin TULUNAY
Supervisor

**Examining Committee Members**

Prof. Dr. Önder Yüksel (METU, EE) _____

Prof. Dr. Ersin Tulunay (METU, EE) _____

Prof. Dr. Nilgün Günalp (METU, EE) _____

Assoc. Prof. Dr. Tolga Çiloğlu (METU, EE) _____

Dr. Hüseyin Yavuz (ASELSAN) _____

**I hereby declare that all information in this document has been obtained and presented in accordance with academic rules and ethical conduct. I also declare that, as required by these rules and conduct, I have fully cited and referenced all material and results that are not original to this work.**

Name, Last name : Süleyman Olcay BÜYÜKPAPUŞÇU

Signature :

## ABSTRACT

### SYSTEM IDENTIFICATION WITH PARTICULAR INTEREST ON THE HIGH FREQUENCY RADAR UNDER IONOSPHERIC DISTURBANCES

**BÜYÜKPAPUŞÇU, Süleyman Olcay**

**M.S., Department of Electrical and Electronics Engineering**

**Supervisor: Prof. Dr. Ersin TULUNAY**

**Co-Supervisor: Prof. Dr. Yurdanur TULUNAY**

**February 2007, 69 pages**

We have been actively involved in the research and management activities of European Co-Operation in the Field of Scientific and Technical Research (EU COST) actions such as COST 238 Prediction and Retrospective Ionospheric Modeling over Europe (PRIME), COST 251 Improved Quality of Service in Ionospheric Telecommunication System Planning and Operation, COST 271 Effects of the Upper Atmosphere on Terrestrial and Earth-Space Communications, COST 296 Mitigation of Ionospheric Effects on Radio Systems (MIERS) and COST 724 Developing the Scientific Basis for Monitoring, Modeling and Predicting Space Weather.

In this thesis High Frequency (3-30 MHz) (HF) radar system under ionospheric disturbances has been identified globally and some operational suggestions have been presented. The use of HF radar system is considered from the identification of ionospheric propagation medium point of view. Doppler velocity is considered as the characteristic parameter of the propagation medium. ap index is chosen as the parameter for disturbance characterization due to geomagnetic storms in the ionosphere.

The main difficulty is the scarcity of data, which is rare and confidential. Therefore semi-synthetic data are generated.

Dependence of Doppler velocity and group range of the echo signal on ap index is examined and some details of dependence are studied and demonstrated.

Thus, effects of space weather on the ionosphere and as a result on HF radar wave propagation are displayed. These results are examples of system identification. This can be used in communication system planning and operation.

Keywords: High Frequency Radar, Ionospheric Disturbances, Ionospheric Backscatter, Magnetic Indices.

# ÖZ

## İYONKÜRESEL DÜZENSİZLİKLER ALTINDA YÜKSEK FREKANSLI RADAR ÖZELİNDE DİZGE TANIYIMLAMA

**BÜYÜKPAPUŞÇU, Süleyman Olcay**
**Yüksek Lisans, Elektrik ve Elektronik Mühendisliği Bölümü**
**Tez Yöneticisi : Prof. Dr. Ersin TULUNAY**
**Ortak Tez Yöneticisi: Prof. Dr. Yurdanur TULUNAY**

**Şubat 2007, 69 sayfa**

Bilimsel ve Teknik Araştırma Alanında Avrupa İşbirliği (EU COST) çerçevesinde gerçekleştirilen araştırma ve yönetim eylemlerinde etkin olarak yer almaktayız. Bu eylemler COST 238 Avrupa Üzerinde Kestirimsel ve Geçmişi İçeren İyonküresel Benzekleme (PRIME), COST 251 İyonküresel Uzaktan İletişim Dizge Planlaması ve İşletiminde Servis Niteliğinin İyileştirilmesi, COST 271 Üst Atmosferin Yersel ve Yer-Uzay İletişimine Etkileri, COST 296 İyonkürenin Radyo Dizgeleri Üzerindeki Olumsuz Etkileri ve En Aza İndirilmeleri (MIERS) ve COST 724 Uzay Havasının İzlenmesi, Benzeklenmesi ve Öngörüsü için Bilimsel Temellerin Geliştirilmesi olarak sıralanabilir.

Bu çalışmada iyonküresel düzensizlikler altında Yüksek Frekanslı (3-30 MHz) (YF) radar dizgesi küresel olarak tanıyımlanmış ve işletim önerileri sunulmuştur. YF Radar dizgesi iyonküresel yayılım ortamı nitelendirilmesi açısından ele alınmıştır. Doppler hızı ortamın belirleyici yayılım özelliği olarak ele alınmıştır. ap dizini manyetik fırtınaların iyonkürede yol açtığı düzensizlikler için bir gösterge olarak seçilmiştir.

Bu çalışmadaki ana güçlük, çok az olması ve gizli olması sebebiyle veri

bulunamamasıdır. Bu nedenle çalışmada yarı-yapay veri oluşturulmuştur.

Doppler hızının ve grup uzaklığının ap dizinine bağlılığı incelenmiştir ve bu bağlılığın ayrıntıları çalışılmış ve gösterilmiştir.

Böylece, uzay havasının iyonküre ve sonuç olarak radar dalga yayılımına etkileri gösterilmiştir. Bu sonuçlar dizge tanıyımlaması için örneklerdir ve iletişim dizge planlama ve işletiminde kullanılabilirler.

Anahtar Kelimeler: Yüksek Frekanslı Radar, İyonküresel Düzensizlikler, İyonküresel Geri Yansımalar, Manyetik Dizinler.

In Loving Memory Of My Father

## ACKNOWLEDGMENTS

I would like to thank my supervisor, Prof. Dr. Ersin Tulunay who has been extremely helpful during the preparation of the thesis.

I would also like to thank my co-supervisor Prof. Dr. Yurdanur Tulunay for her support with her great intelligence and knowledge about the Space Weather.

I would like to acknowledge Assoc. Prof. Dr. Tolga Çiloğlu with appreciation who gave me important clues about data processing.

I would also like to acknowledge Prof. Dr. Nilgün Günalp for her kind help and suggestions during the preparation of the thesis.

I would like to express my gratitude to my mother, Birgül Büyükpapuşçu, my sister, Özlem Büyükpapuşçu, my friend Hanife Yasav, and all colleagues in ASELSAN Inc. who gave me great support during my thesis studies.

## TABLE OF CONTENTS

## LIST OF TABLES

### TABLES

## LIST OF FIGURES

**FIGURES**

## ABBREVIATIONS

HF .....High frequency
OTH ..... Over The Horizon
VLF ..... Very Low Frequency
LF ..... Low Frequency
MF ..... Medium Frequency
LOS .....Line Of Sight
FAI .....Field Aligned Irregularities
IMF .....Interplanetary Magnetic Field
TIGER ..... Tasman International Geospace Radar
SuperDARN .....Super Dual Auroral Radar Network
PRF ..... Pulse Repetition Frequency
UT .....Universal time
QPS ..... Quasi Parabolic Segment
CCIR .....International Radio Consultative Committee
SW ..... Solar Wind
MLT .....Local Magnetic Time

# CHAPTER 1

# INTRODUCTION

## 1.1 Problem Definition

High Frequency (HF) (3-30 MHz) Radar is an important system. HF radars are sometimes called as over-the-horizon (OTH) radars because of their capacity to receive target echoes over much longer distances than microwave radars, which are restricted to distances defined by the line-of-sight or the horizon [1]. The most common type of HF radar operates in the sky wave mode, which receives radar echoes through reflection from the ionosphere. HF radar can also operate in the surface wave mode, which provides coverage in the order of several hundred kilometers [2].

Main HF Radar applications include navigation, reconnaissance and surveillance. HF radar has been used in various fields such as sea transport, disaster management and defense. HF radar is a very important tool for environmental characterizations such as, sea surface characterization, characterization of near Earth space, space weather, ionospheric state and propagation conditions. Communications system planning and operation is possible by the help of the HF Radar.

### 1.1.1. Ionospheric Backscatter

HF Radar can detect direct backscatter from ionospheric irregularities, but it also detects backscatter from signals that are reflected from the ionosphere down to the sea or ground and backscattered, so they return to the radar again via the ionosphere. The characteristics of all these echoes can be used to study the HF propagation. This information can then be used to examine the accuracy of ionospheric models used to predict HF propagation characteristics for HF users.

The echo signal return from the ionospheric irregularities and from ground has characteristic line-of-sight Doppler velocities. E and F region echo velocities are too much higher than the velocities of the echo signal from the Earth surface [3], [4].

Echoes from the ionospheric irregularities have close correlation with geomagnetic activity [4] and the radars tend to observe ionospheric echoes more frequently with the increase of the geomagnetic activity.

In this thesis, effects of space weather on the ionosphere and as a result on HF radar wave propagation are displayed. This can be used in communication system planning and operation.

### 1.2 Scope of the Thesis

In this thesis, HF Channel is considered as a system which involves various physical and chemical processes

The aim of this study is to relate HF radar wave propagation to magnetic indices, which may be considered as the disturbances to the system and give some suggestions for HF radar planning and operation. For this purpose the data which are generated semi-synthetically from an HF Radar experiment is used.

### 1.3 Outline of the Thesis

In Chapter 2, general information about Ionosphere, HF communication, near Earth space and space weather are presented.

In Chapter 3, general information about HF radars and associated terminology, TIGER HF radar, related experiment and ap index are presented. Then the generation of the semi synthetic ionospheric backscatter data is explained.

In Chapter 4, identification of the HF propagation medium under ionospheric disturbance is presented.

In this chapter,

1. The dependencies of ionospheric backscatter observance and the group ranges of these backscatters on ap index is observed.

2. These dependencies are examined in terms of correlation and histogram.

3. By the help of the experimental studies and an ionospheric model, the dependency of the propagation characteristics of the medium on the ap index is presented.

In Chapter 5, some suggestions for the HF radar planning and operation are given by considering the differences between the high latitude, mid-latitude and low latitude ionosphere, ap prediction methods and the seasonal and solar cycle variations of Kp and ap indices.

# CHAPTER 2

# SPACE WEATHER

## 2.1 Ionosphere

The Ionosphere is an upper region of the Earth's atmosphere containing a small percentage of free electrons and ions produced by photo ionization of the constituents of the atmosphere by solar ultra-violet radiation and X-rays. At lower levels of the Earth's atmosphere, radiation has been almost entirely used up so that the degree of ionization is small so, at this level (near the ground), the atmosphere is said to be neutral [5]. That is, it is not ionized and it is comparably almost non-conductive. But at some level neutral density and radiation intensity results the highest ion production rate [6]. This is illustrated in Figure 2-1.

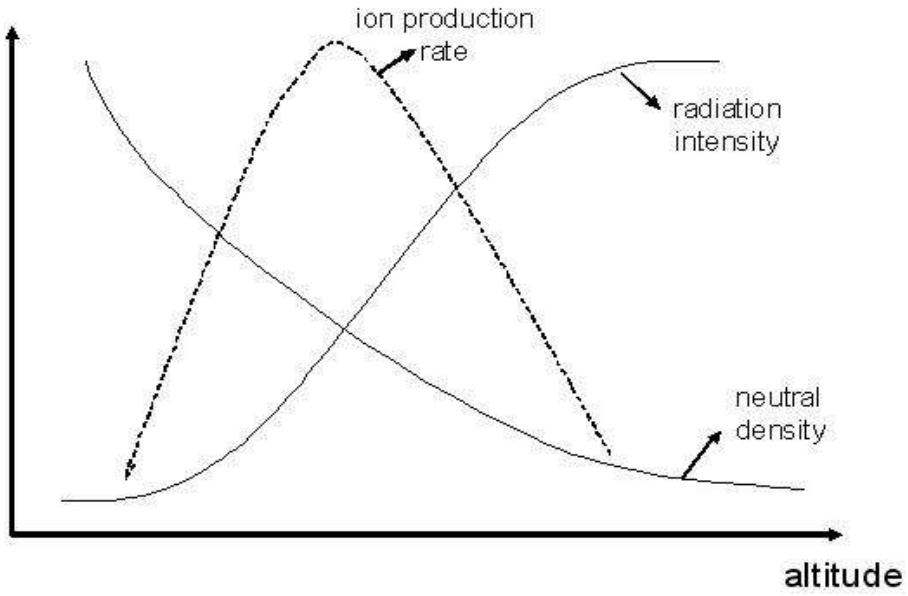


Figure 2-1 Ion Production Rate

### 2.1.1 Ionospheric Layers

The total population of ions and electrons is distributed throughout the ionospheric region. The lower boundary of the ionosphere lies at heights of about 55 km above the Earth. The concentration of electrons increases irregularly, with height to maximum at elevations of 200-600 km, above that, the concentration decreases again, but more slowly and over a much greater height span.

Ionosphere has a layered structure with distinct maxima of electron density occurring in layers called D layer, E layer, F layer and F2 layer [7], [8], [9]. The D region is present only during daytime. The altitude of the peak density is normally around 90 km, but this may decrease to 78 km when the solar X-ray flux is enhanced. The E region peak density occurs at altitude of 110 km. At sunset, the E region electron density drops by a factor of 10 or more in a short period (tens of minutes) before reaching a night time equilibrium density [8]. It mostly disappears but does not vanish at night; a weakly ionized layer remains [9]. The sporadic E region (Es) is transient, localized patches of relatively high electron density in the E region. Es significantly affects radio wave propagation because it may reflect signals that would otherwise penetrate to the F region. Es can occur at almost any time of the day [10]. Very Low and Low Frequency (VLF/LF) waves are reflected from D region during daylight and lower E region at night. On the other hand, at night, Medium Frequency (MF) sky waves can propagate with little attenuation but during the day they are attenuated by the D region [9]. The F region is a combination of two different regions. The F1 region has an altitude peak near 200 km, but is absent at night [8]. The F2 layer has the greatest concentrations of electrons of any layer, and therefore it is the most important region for HF waves [9]. It has a peak near 300 km during the day, and at higher altitudes at night [8].

The electron density profile of the ionospheric layers with additional dependence on diurnal and solar cycle variation is explained in [10] and this situation is illustrated as in Figure 2-2 [10].

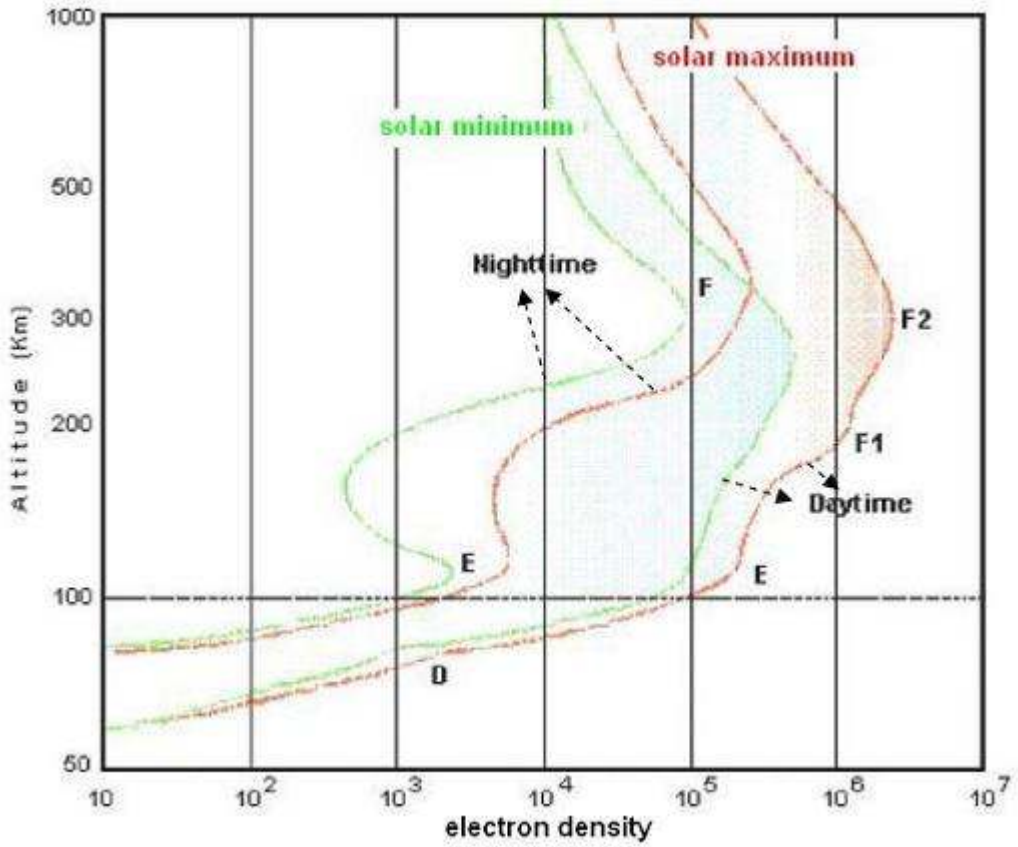


Figure 2-2 Electron Density Profile

## 2.2 HF Communications

The HF band of the electromagnetic spectrum extends from 3 to 30 MHz, corresponding to a wavelength range of 10 to 100m. Radio communications using this frequency band is referred to as HF communications. Many services have frequencies allocated in this band such as Local/International Broadcast, Amateurs, Standard Frequencies, Maritime and Land Mobile, Point-to-Point Communications, Industrial, Scientific, Medical Diathermy, Aero Fixed, Citizens' Band. The band is also used for ionospheric sounding and over-the-horizon surveillance.

### 2.2.1 Ionospheric Propagation

Surface wave, where the waves propagate along the surface of the Earth, and sky wave, where the waves are reflected back to Earth from the ionosphere are the two major propagation mechanisms exist for radio waves in the HF band [11].

Possible propagation paths for HF radio waves are given in [11] as illustrated in Figure 2-3 [11].

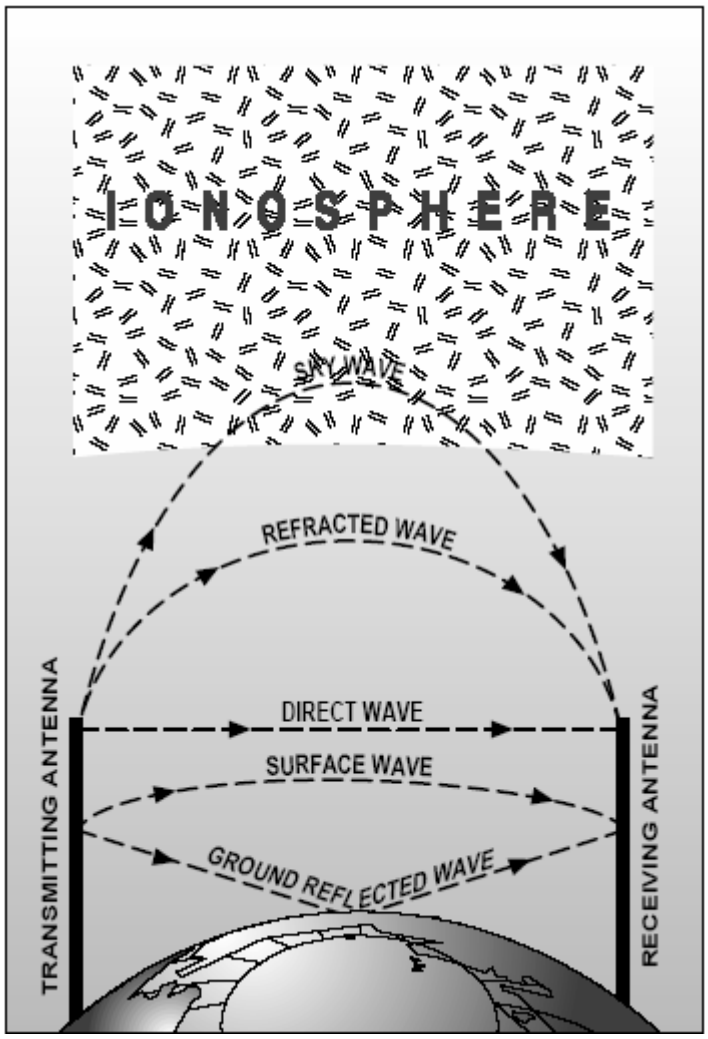


Figure 2-3 Propagation Paths

Some of the terms which are relevant to the subject of this thesis are clarified below::

Propagation in which the direct ray from the transmitter to the receiver is unobstructed is called *Line Of Sight (LOS)* propagation. In other words, the transmission path is not dependent on reflection or refraction. Typically range of LOS is less than 30 km [12]. HF radio waves are capable of propagating beyond the LOS.

HF radars can measure the *LOS Doppler Velocity* of the reflecting media. The Doppler velocities of the reflecting media are calculated by the equation 2-1.

$$V_{doppler} = \left(\frac{c}{2}\right)\left(\frac{\Delta f}{f}\right) \tag{2- 1}$$

where c (m/s) is the speed of light in vacuum, Δf (Hz) is the observed shift in frequency, and f (Hz) is the transmitter frequency [13]. Note that Δf is also called as *Doppler shift*.

For the application of radar, the *group range*, or *group path*, is obtained as follows:

$$GroupRange = \left(\frac{c}{2}\right) \times t_d \tag{2- 2}$$

Where $t_d$ is the time delay of the echo and c (m/s) is the speed of light in a vacuum [14].

The area around a radio station which cannot normally be worked by either ground waves or normal ionospheric sky waves is called as *blind zone* is. This zone is also called the "skip distance" by the US Military [15]. Schematic of the blind zone is shown on Figure 2-4

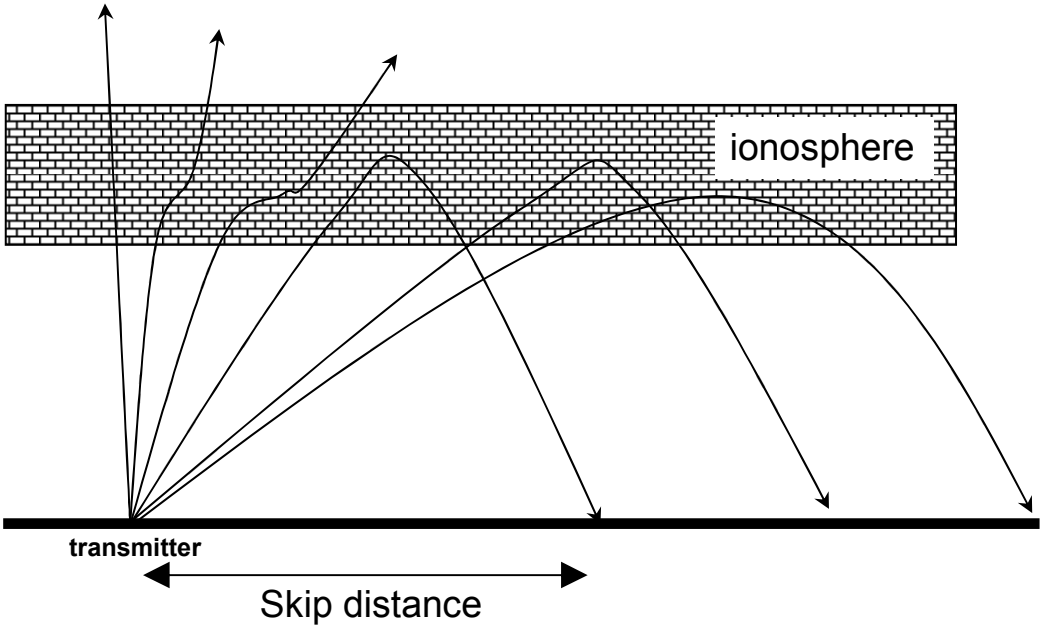


Figure 2-4 Schematic Ray Paths for an Ionospheric Layer

Ionosphere can be grouped in to three parts in latitudes with respect to the geomagnetic activity;

*High Latitude Ionosphere* refers to latitudes between 50° to 80° geomagnetic, *Mid-Latitude Ionosphere* refers to latitudes between 20° to 50° geomagnetic, and *Low-Latitude Ionosphere* refers to latitudes between 0° to 20° geomagnetic [16].

### 2.2.2 Ionospheric Models and Ray Path Calculations

Ionospheric models which give analytical solutions for parameters of the ray tracing algorithms are very useful for HF propagation system planning and operation. Thus, effective modeling of the ionosphere together with accurate ray tracing algorithms is very important for identification of the ionospheric propagation modes.

There are more than fifty HF propagation analysis & prediction software programs which use various ionospheric models. These software programs are

called HF propagation models. The International Reference Ionosphere-2000 (IRI-2000) [17] and Multiple Quasi-Parabolic Segment Model (QPS) [18] are two examples for the ionospheric models and The Voice of America Coverage Analysis Program VOACAP [19] and The Ionospheric Communications Enhanced Profile Analysis and Circuit Prediction Program ICEPAC [19] are two examples of the propagation prediction computer programs.

As an example for modeling of the ionosphere together with ray tracing algorithms, in [20], Nozomu Nishitani and Tadahiko Ogawa calculate the possible ionospheric backscatter echo area for mid-latitude HF radar by using a versatile three-dimensional ray tracing algorithm [21] plus IRI-2001 ionospheric model. Another example is that, in [22], Dyson, Norman and Parkinson showed the synthesized backscatter ionogram of the expected group range of the sea or ground echoes versus frequency. They used the QPS model ionosphere by using the procedures recommended by the International Radio Consultative Committee (CCIR) [23]. A figure of this ionogram will be presented in section 4.3.1.

### 2.3 Near-Earth Space

Near-Earth Space is the space between the Earth and Sun. This space is not empty, but filled with energetic particles, most of which are generated in the solar atmosphere. Temperatures of a few million degrees accelerate a stream of these particles, called the solar wind, to roughly one million miles per hour. Near Earth space processes are highly complex in nature being nonlinear and time varying with the parameters open to the effects of random variations in the Near Earth space such as the solar activities [24], [25]. Near-Earth Space weather phenomena could best be understood by the interaction between the Earth's and Sun's magnetic fields.

Understanding of the Near-Earth Space environment is very important to observe and forecast "space weather" and its effects on space-based and ground-based technological systems [26].

## 2.4 Space Weather

Space Weather is defined by the U.S. National Space Weather Program (NSWP) as: "conditions on the Sun and in the solar wind, magnetosphere, ionosphere, and thermosphere that can influence the performance and reliability of space-borne and ground-based technological systems." [27]. Another definition of the Space Weather is given by The National Oceanic and Atmospheric Administration/Space Environment Center (NOAA/SEC) as a "consequence of the behavior of the sun, the nature of the Earth's magnetic field and atmosphere." [16]. Effects of Space Weather on ground-based systems, satellites and spacecraft systems are briefly summarized in [27].

# CHAPTER 3

# HF RADAR AND GENERATION OF RELEVANT DATA

## 3.1 HF Radars

HF Radars enable the detection of targets beyond the LOS. These radars operate either in sky wave mode or surface wave mode. The former can operate to ranges of 1000-4000 km, the latter operates to ranges of 10-400 km. Applications of HF radars include ship detection, aircraft detection, iceberg detection, repeater tracking and remote sensing of sea surface currents, winds and waves [28] and also ionospheric irregularities.

### 3.1.1 History

German physicist Heinrich Hertz discovered electromagnetic waves in 1887. The principle behind radar based on the electromagnetic wave propagation was described by the American Hugo Gernsback in 1911 [29]. In 1931, Butement and Pollard proposed a coastal defense radar system to the British War Office [30]. Radar was used successfully for the first time to detect aircraft in 1934 by the French scientist Pierre David [29].

In 1937, the first operational HF radars of the Chain Home series were demonstrated by UK and they played an important role during World War II for the air defense of Britain during the war. HF radars indicated returns from extreme ranges, due to ionospheric reflection beyond the horizon. But they were designed as line-of-sight radars and long-range backscatters from the distant ground via an ionospheric reflection were generally only a source of confusion [30]. So, instead of considering its usefulness, it was actually considered a national security risk and radar systems had to be quickly relocated to frequencies free from backscatter

because backscatter causes false indications of a missile attack [13].

After the World War II, US Naval Research Laboratory experimented in HF radar considering the ionospheric propagation and recognized that HF radars can be useful for the discrimination of targets against the inevitable ground backscatter must be provided through signal processing and towards the end of 1961; their works resulted in the first HF radar detections of air targets [30]. In addition to this, in the early 1990's, many HF military radar systems were transformed into HF Doppler weather radar stations and used to search the mechanism of backscatters from ionosphere [13].

### 3.1.2 HF Radar and Associated Terminology

To understand the space weather it is necessary to develop and deploy observational techniques that can observe large areas in the ionosphere. HF radar, operating in the sky wave mode is one such technique [31].

Because of the dynamic nature of the high-latitude ionosphere, small-scale (<100m) ionospheric irregularities, which are aligned along the Earth magnetic field direction, occur and these irregularities cause the HF radio waves to backscatter [22]. But, for an HF radar wave to backscatter; the ray must be perpendicular to the local magnetic dip angle. HF Radars can detect echoes backscattered by these irregularities whenever they occur within the radar beam. [22].

HR radar signal is refracted and partly backscattered by the small- scale electron density irregularities in the ionosphere as shown in Figure 3-1 [22], [32]. Since at high latitudes the Earth's magnetic field lines are almost vertical, ionospheric scatter echoes are detected by HF radars at ranges approximately equal to 0.5 and 1.5 times the range of backscattered ground or sea single hop echoes as shown in Figure 3-2 [31].

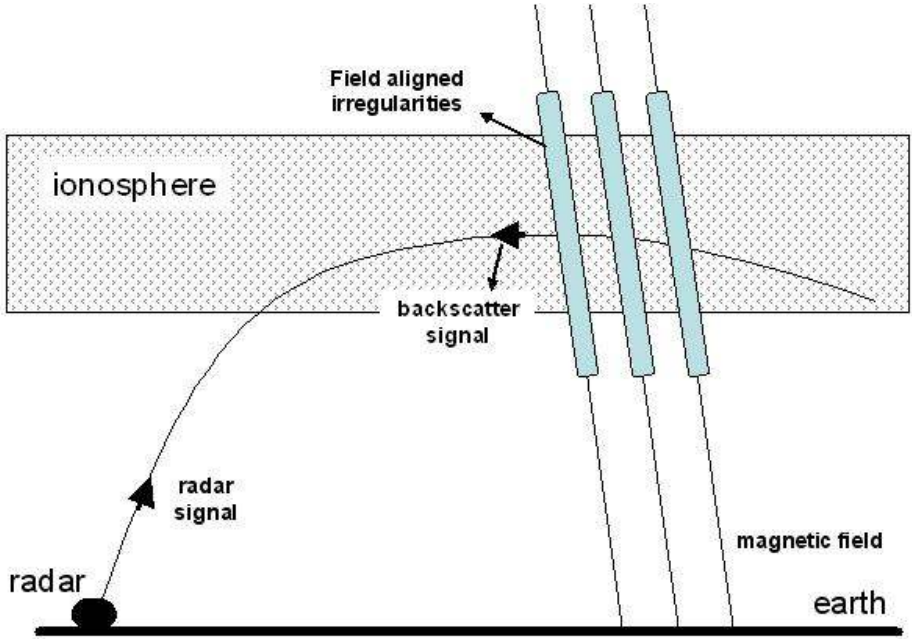


Figure 3-1 Principle of the HF Radar

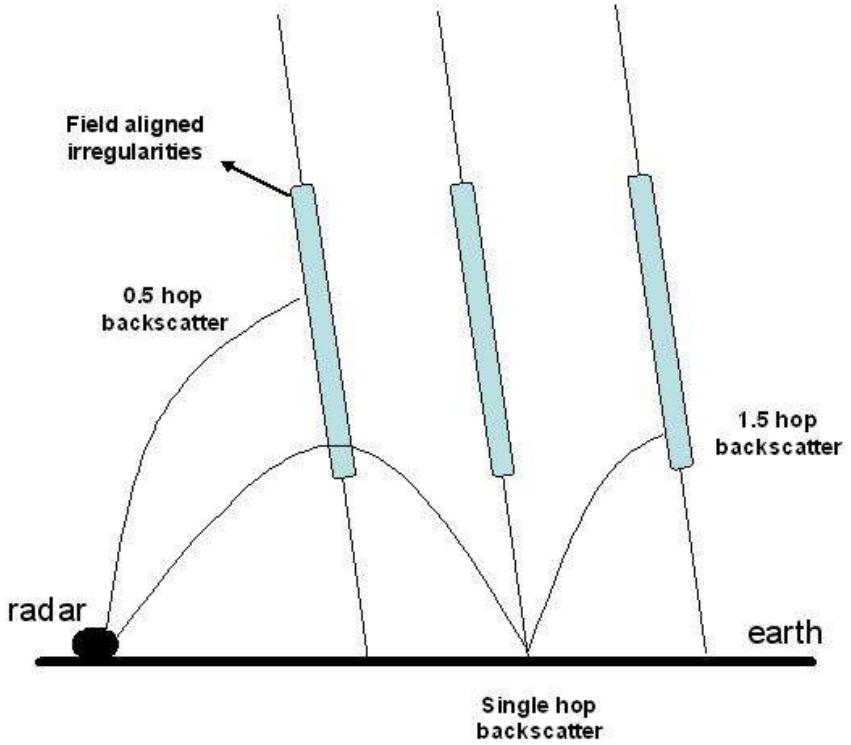


Figure 3-2 Possible Ray Paths of HF Radar Wave

Another important factor which affects the observance of ionospheric backscatter is the presence and absence of ionospheric field-aligned irregularities (FAI) of the spatial scale of λ/2, where λ is the wavelength of the radar HF wave [20]. This condition is illustrated in Figure 3-3. Without this spatial scale, the radar HF waves are not backscattered even if the perpendicularity condition is satisfied in the ionosphere [31].

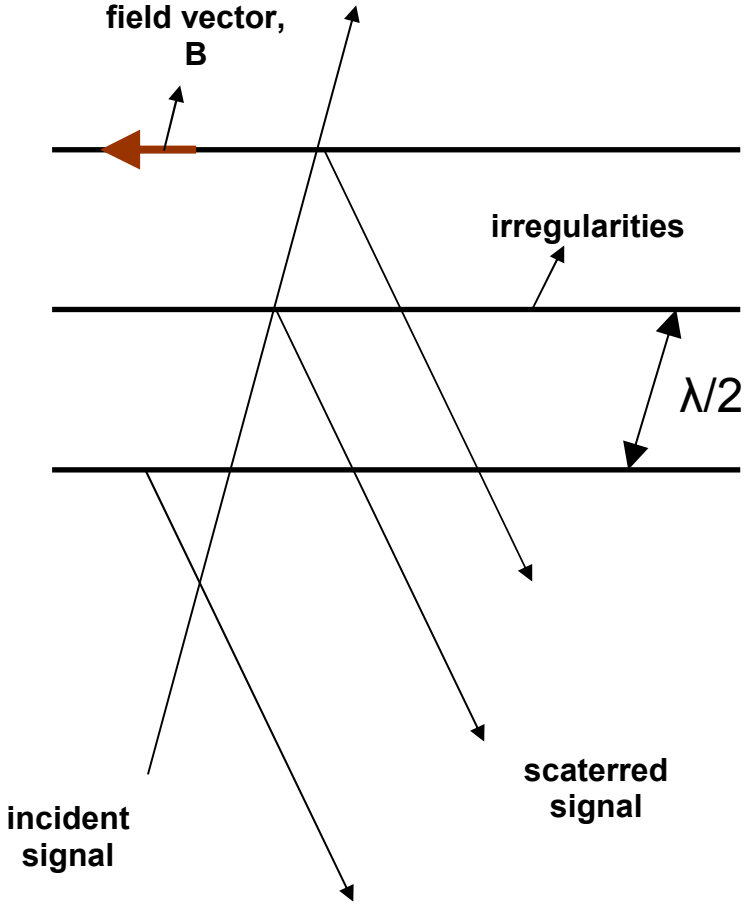


Figure 3-3 Radar Scatter from Ionospheric Irregularities

Normally, the HF radars measure the velocity of these FAIs. So the ionespheric backscatter occurrence gives important information about the distribution of FAIs and their generation mechanisms [3]. The subauroral F region ionosphere is one of the active sources of FAIs and therefore a good target for coherent scatter radars [45].

The complex interaction of the solar wind and Interplanetary Magnetic Field (IMF) with the magnetosphere causes a wide variety of phenomena. As the solar wind blows across the connected field lines, a current is generated and the magnetic field lines provide excellent conduction paths down into the ionosphere, allowing the current to discharge through the high-latitude ionosphere [31].

The electric field across the magnetosphere is directed from dawn to dusk and, causes an $\overline{E}X\overline{B}$ convection flow in the ionosphere [4]. As discussed in [3] and [4] at the high latitude F region, velocity of the FAIs is in the direction of $\overline{E}X\overline{B}$ and proportional to:

$$\frac{\overline{E}X\overline{B}}{\overline{B}.\overline{B}} \qquad (3\text{- }1)$$

During geomagnetic disturbances, the electric fields and particle populations which characterize the auroral region expand equatorward and their effects are felt at previously subauroral latitudes. Ionospheric backscatter echoes detected from these regions have characteristic Doppler shifts indicative of the FAIs [33].

### 3.2 TIGER HF Radar

#### 3.2.1 Radar Information

The Tasman International Geospace Environment Radar (TIGER) is dual HF ionospheric radar system operating at oblique incidence. These HF Radars examine the ionosphere between Tasmania and Antarctica [31]. TIGER can detect direct

backscatter from ionospheric irregularities as well as detects echoes from signals that are reflected from the ionosphere down to the sea, and then backscattered [22].

TIGER is a part of the Super Dual Auroral Radar Network (SuperDARN). SuperDARN is a global-scale network of HF and VHF radars [34]. These radars are capable of sensing backscatter from ionospheric irregularities in the E and F-regions of the high-latitude ionosphere [35]. SuperDARN radars probe the southern and northern high-latitude ionospheres to study the high-latitude ionosphere [22]. TIGER is located at lower geomagnetic latitude than other SuperDARN radars. So, it can extend the SuperDARN technique to the subauroral region [31].

The first TIGER radar is installed at Bruny Island, Tasmania (147.2°E, 43.4°S, geographic; -54.6°Λ geomagnetic) and it has been operational since November 1999 [22]. It is also called as TIGER-Bruny Radar. The second one is located on the South Island of New Zealand near the city of Invercargill (167.7°E, 46.2°S, geographic), began operation in November 2004. It also called as TIGER-Unwin Radar [36], [37].

Figure 3-4 shows the field of view of the TIGER radars. This figure is taken from [31] and [38]. The straight lines show the 16 azimuthal directions scanned by the ~3° azimuthal beam of each radar. The solid curved lines show the geomagnetic latitudes whereas; the dotted lines show the geographic latitude and longitude [38].

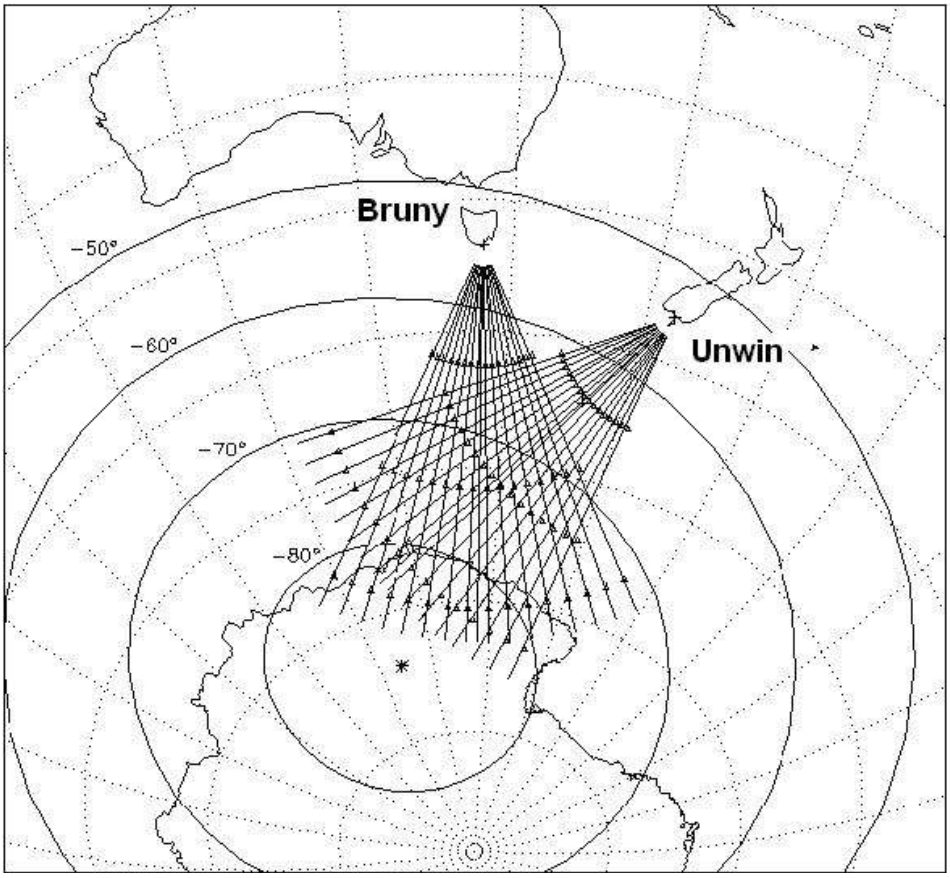


Figure 3-4 Field of View of the TIGER Radars

Radars use an array of 16 log-periodic antennas and cover 52º of azimuth by sequentially stepping through 16 beam directions [39].

TIGER Radar specifications are given in Table 3-1 [38].

Table 3-1 TIGER Radar Specifications

| | |
|---|---|
| **Frequency Band** | 8 – 20 MHz |
| **Antenna Arrays** | Tx/Rx Array: 16 horizontally polarized log-periodic |
| | 2nd Rx Array: 4 horizontally polarized log-periodic |
| **Beam Widths** | Horizontal: $4^{o}$ at 10 MHz, $3^{o}$ at 14 MHz, $2^{o}$ at 18 MHz |
| | Vertical: $50^{o}$ |
| **Lobe Levels** | < -14 dB for both back and side lobes |
| **Transmitters** | 16 x 600 W (one per antenna in Tx/Rx array) |
| **Total Peak Power** | 9.6 kW |
| **Mean Power** | 200 W |
| **Radiated Power** | 12.5 W in main beam direction |
| **Tx signals** | Pulse pattern repetition rate: 50 or 100 ms |
| | Pulse width 300 μs |
| | Bandwidth 10 kHz at –20 dB |
| | Duty cycle 2.1% |
| | Carrier frequency stability better that $10^{-8}$ per day |

### 3.2.2 TIGER HF Radar Experiment

TIGER Radars are much closer to the south magnetic pole than the south geographic pole. Because of the locations, radars are appropriate to monitor the interaction of the Solar Wind with the Earth's magnetic field [36].

TIGER radars can detect small-scale magnetic field-aligned ionospheric irregularities in the high-latitude ionosphere as well as backscatter from the Earth's surface [37]. Radars are capable of determining the echo power, group range, Doppler spectrum, and the azimuth and elevation angles of arrival [31].

Radars can operate in the frequency range 8–20 MHz, but due to both license restrictions and determine the interference free frequency band, operation frequency change automatically to provide the best coverage of ionospheric scatter [37], [31]. In this thesis, data from the Bruny Radar are used. For the dates which are used in

this thesis, Bruny Radar operates mainly at two frequency bands; about 11 MHz and about 14 MHz.

TIGER is a pulse radar [38] and use short pulses to obtain high range resolution but the pulse repetition frequency (PRF) is limited by the range ambiguity [28]. It means that if the PRF is lower, the range the radar identify the echo velocity is greater, but a low PRF, will cause aliasing of the Doppler spectrum and ambiguity in the determination of echo velocities [38].

Ionospheric velocities cause Doppler shifts higher than 100 Hz, requiring the radar to sample at least at 200 Hz. If a regular pulse train is used, the corresponding range window would be 750 km. This range is very short, because many echoes are returned from distances up to 2000 km [31]. So TIGER Radars must use lower PRF. TIGER Radars use a sequence of pulses as shown in Figure 3-5 at different spacing that are multiples of a minimum spacing to overcome the range-Doppler ambiguity [38].

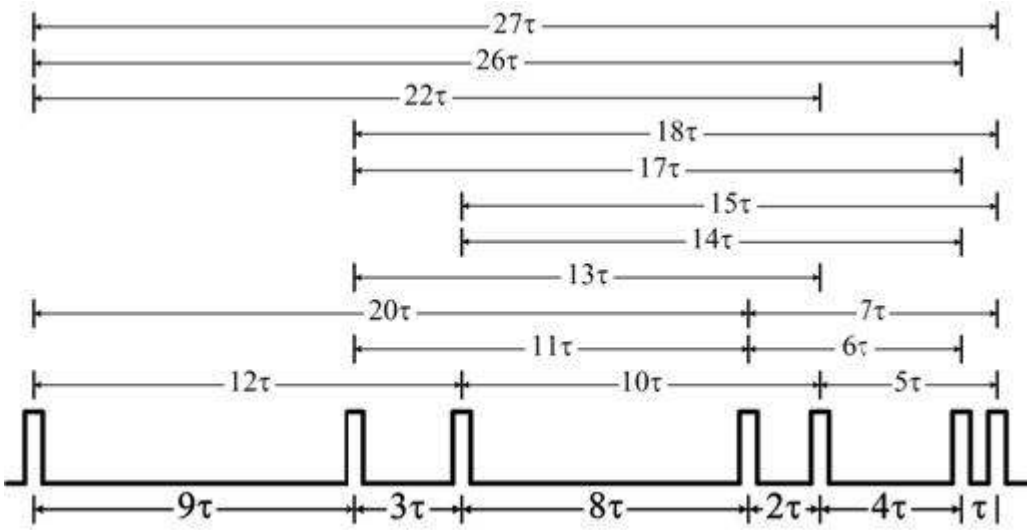


Figure 3-5 TIGER Radar Pulse Sequence

The pulse integration time is commonly 7 s [31] and the pulse length is about 100 ms [38]. Radars can calculate the autocorrelation functions of echoes with 75 range gates starting at 180 km and separated by 45 km [37] by means of the 16 element transmit/receive antenna [31]. Radars also calculate the cross correlation functions for the echoes detected with the 4 element receive-only antenna [31]. Thus, radars can estimate the echo power in logarithmic units of signal-to-noise ratio (dB), LOS Doppler velocity (m/s), and the Doppler spectral width (m/s), for all ranges on every beam [37]. The Doppler velocity characteristics of the echoes are used to determine whether they come from the sea or ionosphere [31].

Figure 3-6, taken from the open source [40], shows a daily summary plot of echo power, LOS Doppler velocity and Doppler spectral width for the single antenna beam direction of Bruny Radar on 13 May 2001.

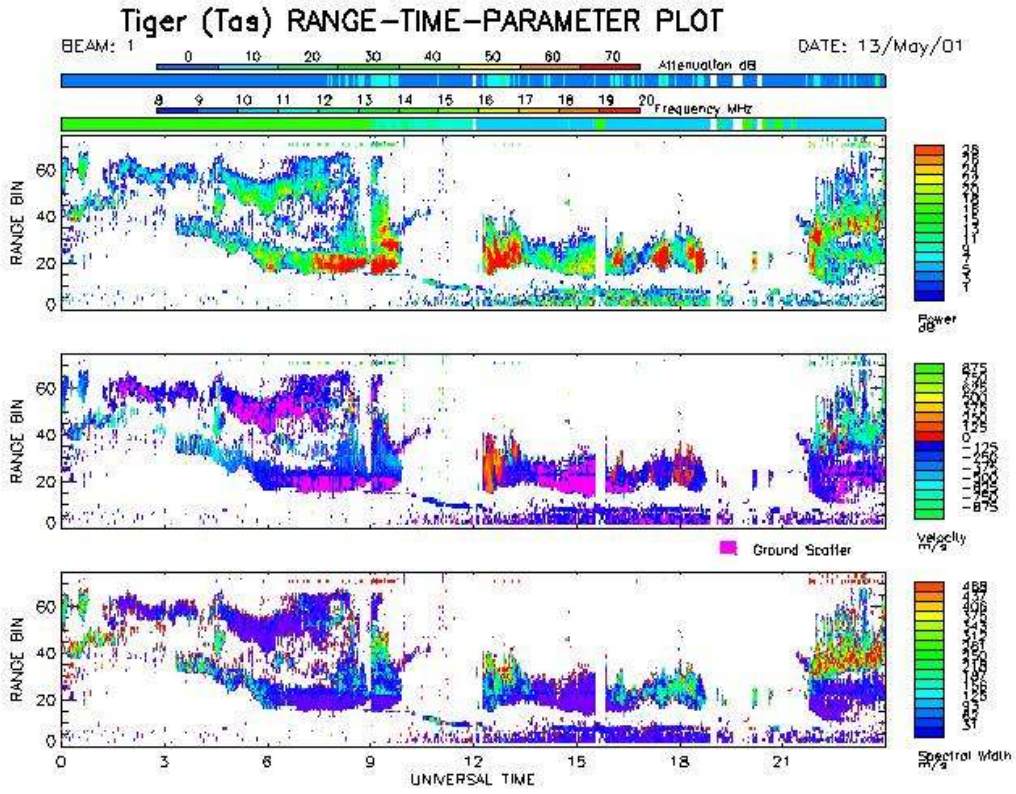


Figure 3-6 Bruny Radar Summary Plot on 13 May 2001

The range scale of the plots in Figure 3-6 is given in range bins, where one range bin equals to 45 km. The time scale is given in Universal Time (UT).

## 3.3 Generation of Semi-Synthetic Data

### 3.3.1 Ionospheric Backscatter

F layer is very important for shortwave communication and the HF sky wave radar, and in most cases it is the reflection layer for long distance communication [41]. In addition to this, F layer is one of the most important layers of the ionosphere as far as scattering is concerned. Irregularities in the F layer are magnetic-field aligned and scattering from these irregularities is strongest when the incident beam is perpendicular to the magnetic field [42], [43]. This perpendicularity often occurs because of refraction of the radio beam in the F layer [42].

When the HF radar is considered, the main difficulty is the scarcity of data, which is rare and confidential. Since, we could not obtain the raw data from the TIGER HF Radar experiment, semi-synthetic data are generated from the TIGER summary plots.

From now on, throughout the thesis, only the Bruny Radar is considered.

Summary plots (i.e., Figure 3-6) contain three figures; each of them contains range bin-time-parameter plots. From the top plot to bottom plot, the parameters are echo power, echo velocity and echo spectral width respectively.

As discussed in Section 1.1.1, the echo signal return from the ionospheric irregularities and from ground has characteristic LOS Doppler velocities. F-region echoes have velocities up to 875m/s and velocity of the E-region echoes is up to 200m/s. On the other hand, ground backscatter LOS Doppler velocities are less than 50m/s [3], [4]. In addition to this, ionospeheric echoes have higher Doppler spectral width than the ground echoes, i.e., Doppler spectral width of the ground echoes are

typically less than 20m/s [39]. So, it is possible to differentiate the backscatter from ionosphere to backscatter from surface of the Earth whenever it occurs in a radar beam.

The parameters in the range bin-time-parameter plots are the third dimension of the plots and shown with the color bars. LOS Doppler velocity change between -875 m/s to +875 m/s with respect to the color bar in the plot. Positive Doppler velocity means the scaterrer moves toward the radar and negative means away from the radar [44], [45]. The sign of the Doppler velocity does not affect the determination of the ionospheric backscatter.

F layer is very important for HF radar applications. Magnetic field lines are vertical in the high latitude ionosphere and the irregularities are field aligned in the F layer. Thus, in this thesis, backscatter signals from F layer take an important role for the identification of the propagation medium.

But the main constraint for the generation of semi-synthetic ionospheric backscatter data is the resolution of the figures and the step size of the color bar. Thus, velocities higher than ~ (+250) m/s and lower than ~ (-250) m/s can be distinguished from the velocities of the backscatters from the Earth surface and from the E layer. The color bar is in 125 m/s steps, therefore by considering the error of the velocity measurement, velocities higher than ~ (+190) m/s and lower than ~ (-190) m/s can be distinguished from the velocities of the backscatters from the Earth surface and from the E layer.

Since the radar can calculate the group ranges of echoes with 75 range gates starting at 180 km and separated by 45 km, error of the group range measurement is approximately ± 25 km and the calculated group ranges from the summary plot is given below:

$$group\_range = (range\_gate) * 45 + 180 \pm 25 \,(\text{in km}) \qquad (3\text{-}2)$$

Since, in this thesis only the range bin-time-echo velocity plot is considered, Figure 3-7 shows the range bin-time-echo velocity plot of the Figure 3-6.

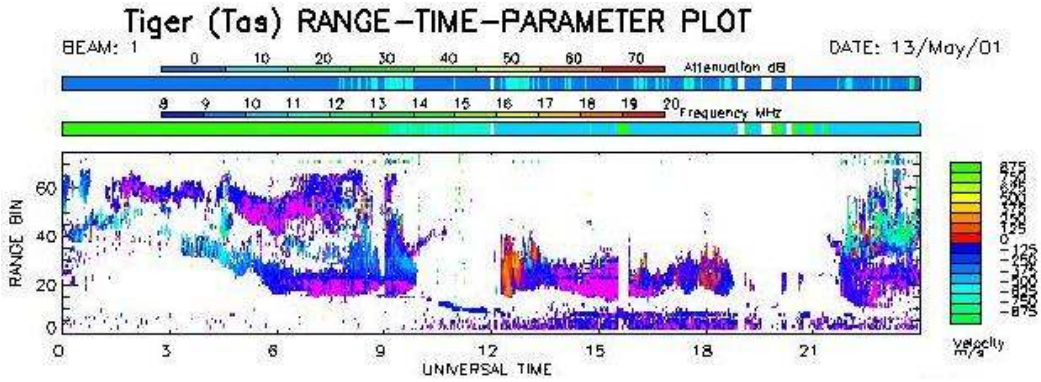


Figure 3-7 Bruny Radar Echo Velocity Plot on 13 May 2001

When the signatures of the echo velocities between (+190) m/s and (-190) m/s are excluded from the figure and the figure is plotted again, Figure 3-8 is obtained. Note that, Figure 3-8 contains only the signatures of the echo velocities higher than (+190) m/s and lower than (-190) m/s.

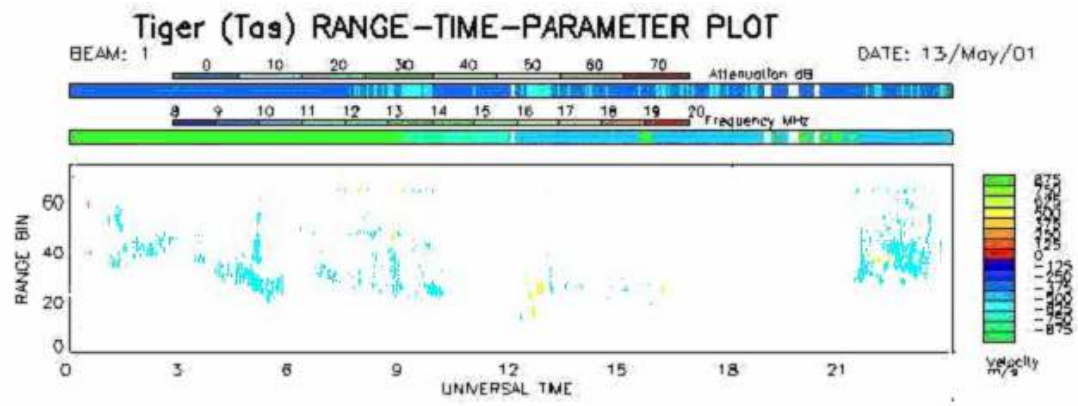


Figure 3-8 Bruny Radar Filtered Echo Velocity Plot on 13 May 2001

From Figure 3-8, we can conclude that, a patch of ionospheric echoes between the group ranges of approximately 1950-2900 km is evident from 23-24 UT. A patch of ionospheric echoes between the group ranges of 1050-2630 km is also evident from 04-05 UT. But, the intensity of the color indicates that number of ionospheric echoes between 22-24 UT is higher than the number of ionospheric echoes between 04-05 UT.

For identification of the intensity of the color, in other words, the number of ionospheric echoes, the number of pixels of the colored (i.e., not white) area inside the red rectangle of Figure 3-9 can be counted. The result gives a symbolic number which accounts for the "number of ionospheric backscatter observance". For simplicity and convenience, the result can be grouped in 1h interval. Therefore, for one day duration, an array consisting of 24 elements is constructed.

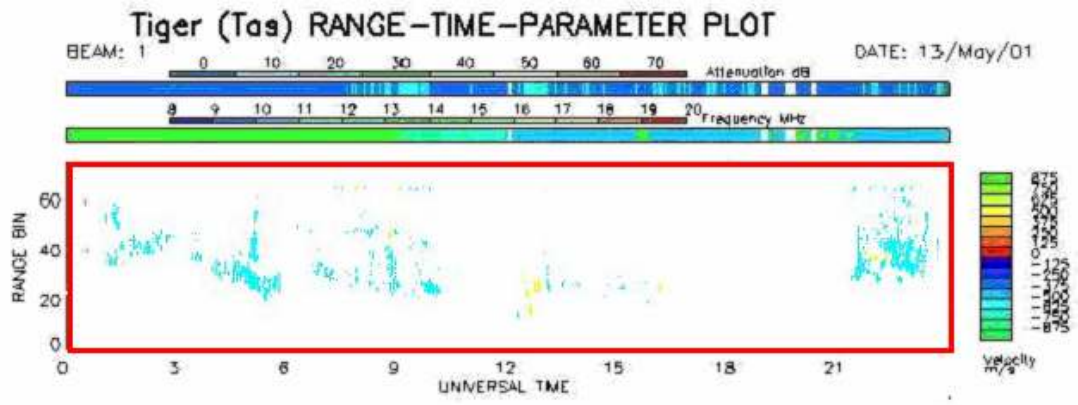


Figure 3-9 Bruny Radar Filtered Echo Velocity Plot-2 on 13 May 2001

The difference in the number of ionospheric backscatter observance for the two different hour interval can be understood better as follows;

Figure 3-10 shows the plot of the number of ionospheric backscatter observance for 13 May 2001 with respect to the UT. For example, the value of the number of ionospheric backscatter observance at 05 UT is 242. It means that there are number of 242 colored pixels from 04-05 UT. But there are number of 332 colored pixels from 23-24 UT.

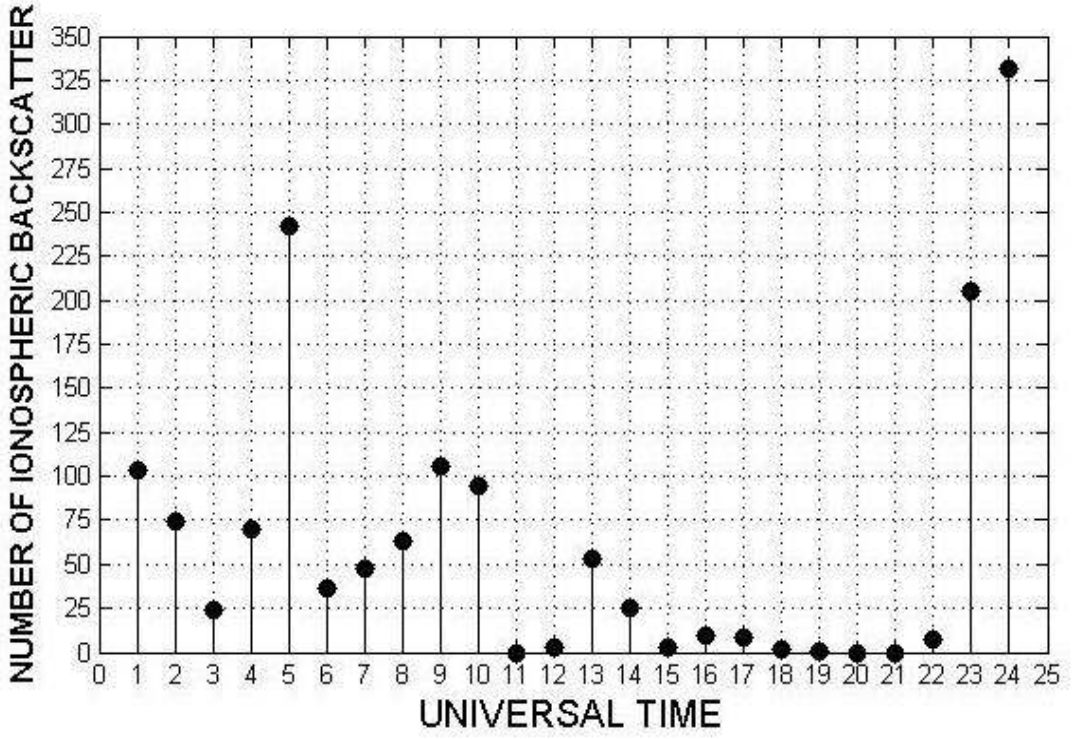


Figure 3-10 Number of Ionospheric Backscatter Observance on 13 May 2001

In this thesis, summary plots from [40] for 335 days between 29 March 2001 and 26 February 2002 are used for data analysis. Since between 13 August 2001 and 22 August 2001 and between 8 February 2002 and 11 February 2002 is missing in [40], the data base of this thesis contains 321 days.

Plot of the number of ionospheric backscatter observance for this interval is shown in Figure 3-11.

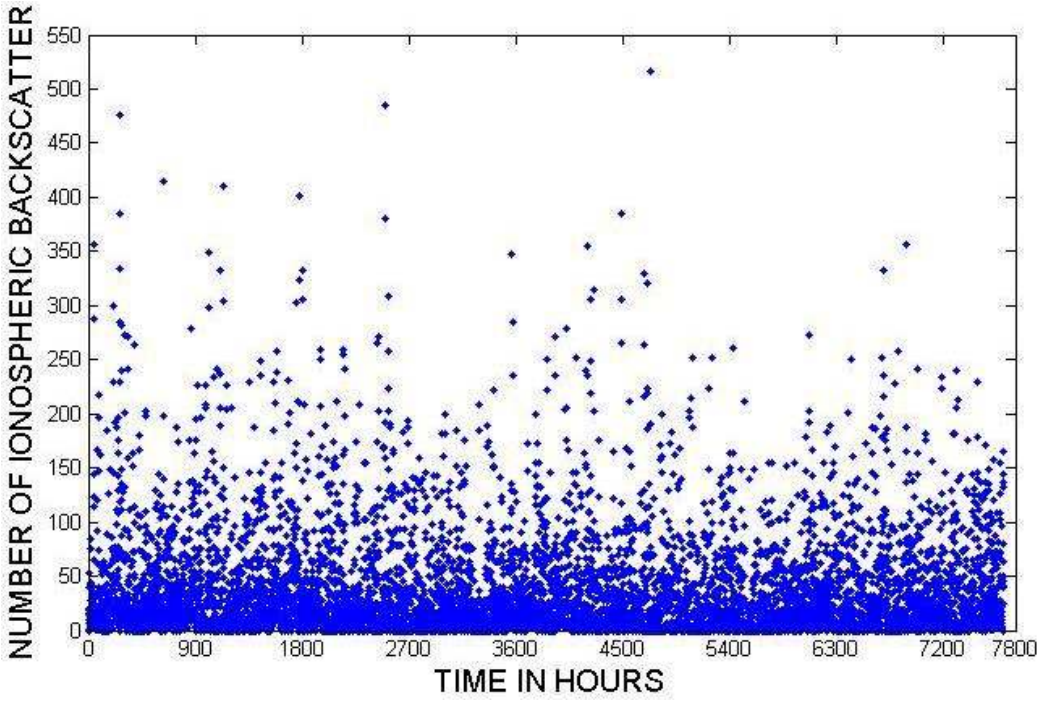


Figure 3-11 Number of Ionospheric Backscatter Observance for 321 days

### 3.4 ap Index

The use of indices of geomagnetic activity plays an important role in the study of solar-terrestrial relationships [46]. Magnetic activity indices were designed to describe variation in the geomagnetic field [47]. The most commonly used indices are AE, Dst, Kp and ap the linear counterpart of Kp [46].

The Kp index represents the intensity of planetary magnetic activity as seen at subauroral latitudes [47] and is the planetary 3-hour-range index from 13 geomagnetic observatories between 44 degrees and 60 degrees northern or southern geomagnetic latitude [46].

Because of its wide usage [48] Kp as well as the ap index is appropriate for this thesis. For convenience, in this thesis ap index is used instead of Kp, since ap is based on a linear scale, whereas Kp is on a quasi-logarithmic scale. ap index is

obtained from [49].

The scale of Kp is 0 to 9 expressed in thirds of a unit, for example 4- equals to (4 - 1/3), 4o equals to 4 and 4+ equals to (4 + 1/3). The 3-hourly ap index is derived from the Kp index as shown in Table 3-2 [47]:

Table 3-2 Kp and ap Conversion Table.

| **Kp** | 0o | 0+ | 1- | 1o | 1+ | 2- | 2o | 2+ | 3- | 3o | 3+ | 4- | 4o | 4+ |
|---|---|---|---|---|---|---|---|---|---|---|---|---|---|---|
| **ap** | 0 | 2 | 3 | 4 | 5 | 6 | 7 | 9 | 12 | 15 | 18 | 22 | 27 | 32 |

| **Kp** | 5- | 5o | 5+ | 6- | 6o | 6+ | 7- | 7o | 7+ | 8- | 8o | 8+ | 9- | 9o |
|---|---|---|---|---|---|---|---|---|---|---|---|---|---|---|
| **ap** | 39 | 48 | 56 | 67 | 80 | 94 | 111 | 132 | 154 | 179 | 207 | 236 | 300 | 400 |

Plot of the ap data for 321 days duration is shown in Figure 3-12.

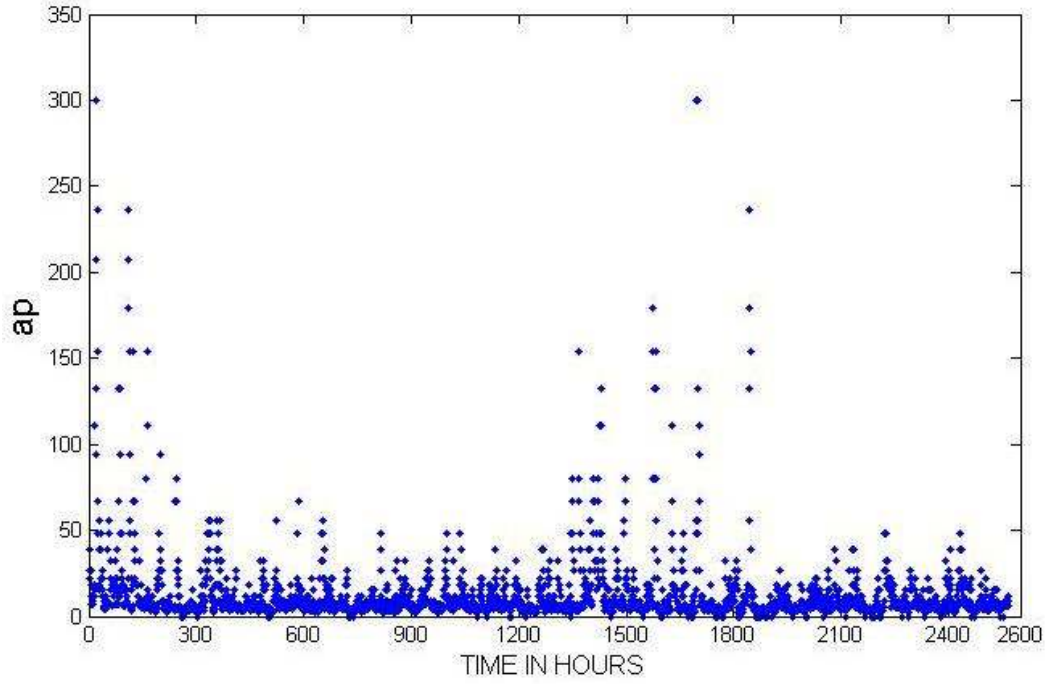


Figure 3-12 ap Data for 321 Days

# CHAPTER 4

# IDENTIFICATION OF THE HF PROPAGATION MEDIUM UNDER IONOSPHERIC DISTURBANCES

## 4.1 Introduction

The location and the distribution of the ionospheric backscatter depend on the ionospheric disturbance conditions [31]. The situation can be utilized to study the effects of the ionospheric disturbance and the properties of the ionosphere used in making ionospheric predictions for users of the HF spectrum [22].

ap index is chosen as the parameter for ionospheric disturbance as stated in section 3.2.2. Therefore, location and the distribution of the ionospheric backscatter are examined with geomagnetic index ap.

## 4.2 Ionospheric Backscatter Dependency on the ap Index

Correlation between ap index and number of ionospheric backscatter observance is studied using both the Pearson correlation method and histograms. Correlation and histograms used for the 321-day length data.

### 4.2.1 Correlation

A physical relationship between two different variables can be estimated by the Pearson correlation method. This method calculates the linear correlation coefficient “r”. This coefficient indicates whether or not the two indices are linearly related [46].

Linear correlation coefficients with respect to time lags between ap index and 3-hour averaged number of ionospheric backscatter observance is shown in Figure 4-1.

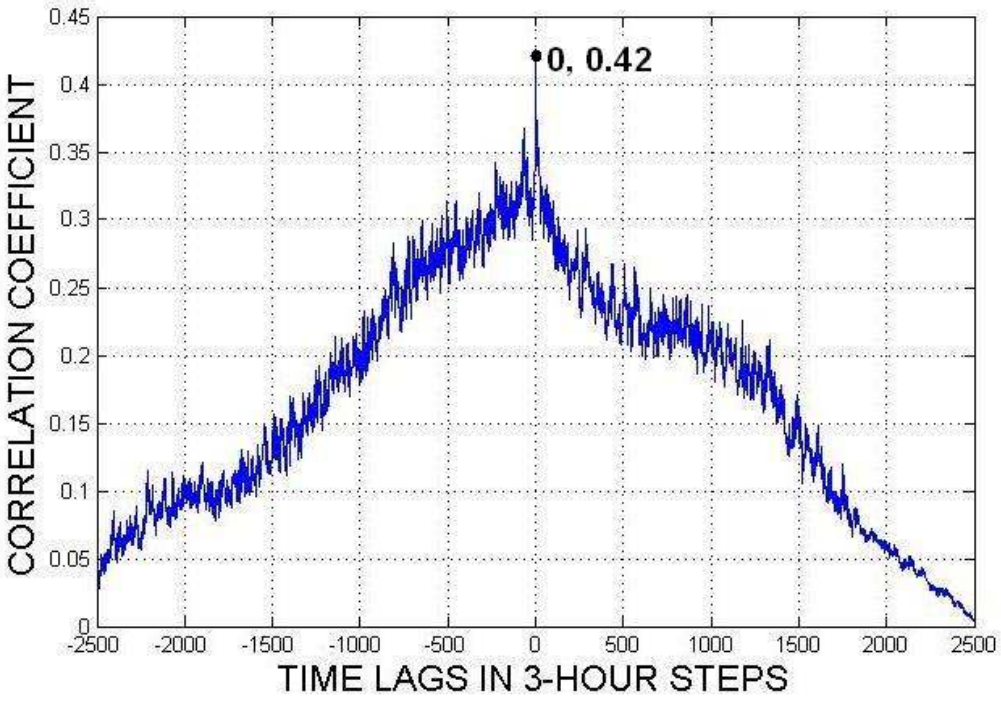


Figure 4-1 Cross Correlation of ap and Number of Ionospheric Backscatter Observance

Maximum linear correlation coefficient occurs at zero time lag and takes the value of 0.42. Since the value of maximum correlation coefficient is small, we can conclude that there is no linear correlation between the ap index and the number of ionospheric backscatter observance. But the figure indicates that there is no time lag between the two parameters when the correlation coefficient takes the maximum value.

### 4.2.2 Histograms

Figure 4-2 shows the distribution of ap versus number of ionospheric backscatter observance.

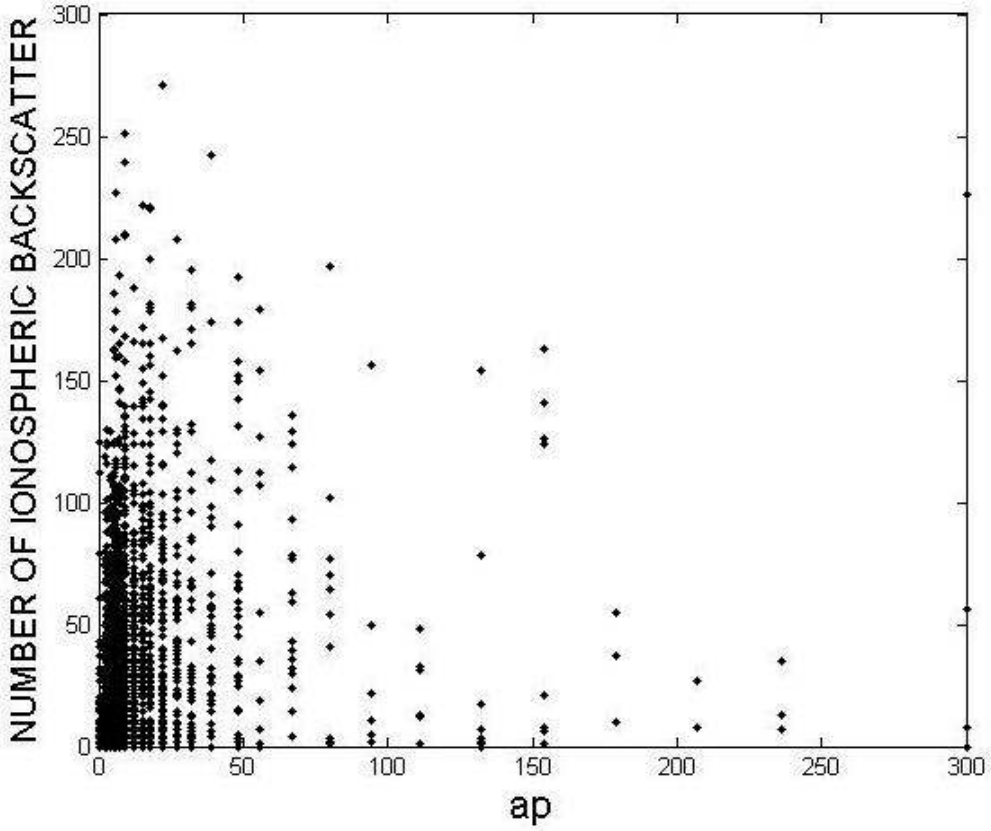


Figure 4-2 ap vs Number of Ionospheric Backscatter Observance

As shown in Figure 4-2, distribution is very intense at ap values between 0-18. But, actually ap values very often stay between 0-18 in real time. This situation is given in Figure 4-3, the histogram of the ap values. Therefore, this distribution does not give any idea about the appropriate solution of relation between the ap and the number of ionospheric backscatter observance. It is necessary to take into account the distribution of ap index for 321-day duration. Distribution of the ap index for 321 days means the histogram of the ap index for this duration.

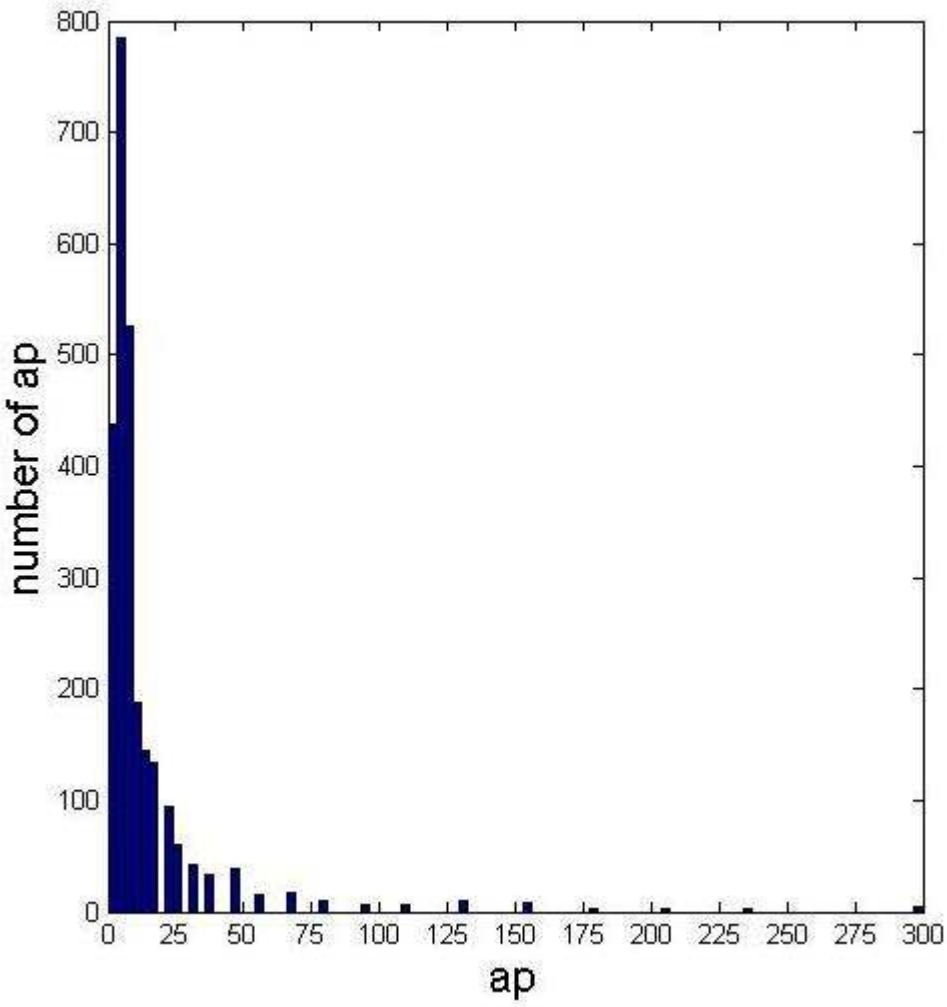


Figure 4-3 Histogram of ap Index in 321-Day Duration

ap versus number of ionospheric backscatter observance will be re-plotted with the procedure explained as follows;

1) With respect to the distribution of ap values given in Figure 4-3, ap data can be grouped in 14 distinct values as shown in Table 4-1.

Table 4-1 Grouped ap Data

| **Index no** | **ap index** | ***grouped_ap*** |
|---|---|---|
| 1 | 0 | 0 |
| 2 | 2 | 2 |
| 3 | 3 | 3 |
| 4 | 4 | 4 |
| 5 | 5 | 5 |
| 6 | 6 | 6 |
| 7 | 7 | 7 |
| 8 | 9 | 9 |
| 9 | 12 | 12 |
| 10 | 15 | 15 |
| 11 | 18 | 18 |
| 12 | 22, 27 | 24.5 |
| 13 | 32, 39, 48 | 40 |
| 14 | 56, 67, 80, 94, 111<br>132, 154, 179, 207<br>236, 300, 400 | 140 |

Note that, by considering the distribution of the ap values in 321-day duration as shown in Figure 4-3, ap values from 0 to 18 are taken one by one, but the remaining ap values are grouped in i.e., 2, 3 and 12 values by trial and error method. Resulting *grouped_ap* values are shown in Table 4-1. *grouped_ap* values are calculated as follows.

$$grouped\_ap = \frac{(\text{summation of the corresponding ap values})}{(\text{number of ap values used in the summation})} \qquad (4\text{- }1)$$

Note also that, *grouped_ap* values are the averages of the corresponding ap indices.

2) Each number of ionospheric backscatter observances which corresponds to each distinct grouped ap values are summed up. This value is called as

*total_backscatter*. Then this value is divided by the corresponding number of grouped ap values in the data set. This value is called as *averaged_backscatter*. *averaged_backscatter* values are calculated as follows.

$$averaged\_backscatter = \frac{total\_backscatter}{(\text{number of corresponding } grouped\_ap \text{ values})} \quad (4\text{-}2)$$

Table 4-2 shows some sample data from step-2.

Table 4-2 Sample Data

| *grouped_ap* | # of *grouped_ap* | *total_backscatter* | *averaged_backscatter* |
|---|---|---|---|
| 0 | 74 | 1033 | 13.96 |
| 12 | 188 | 6552 | 34.85 |
| 40 | 115 | 7050 | 61.3 |
| 140 | 84 | 4313 | 51.35 |

Figure 4-4 shows the distribution of *grouped_ap* versus *averaged_backscatter*.

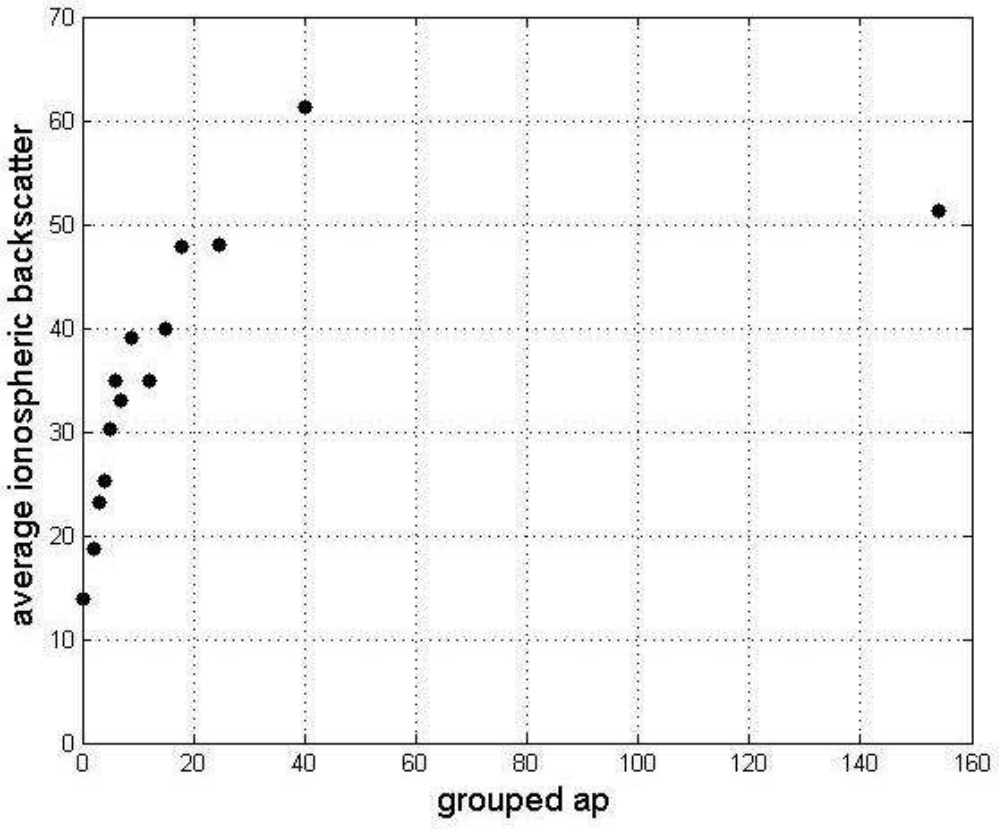


Figure 4-4 *grouped_ap* versus *averaged_backscatter* Observance

Figure 4-4 clearly explains that there is some relation between the ap index and number of ionospheric backscatter occurrence. That is; as the ap index increase, number of ionospheric backscatter occurrence increases. In other words, when the ionosphere is disturbed by magnetic activity, it is more probable to observe ionospheric backscatter for the Bruny HF radar.

### 4.3 Identification of the Propagation Medium

In this section, ionospheric backscatters from 30 days Bruny Radar summary plots will be worked for localization purposes with respect to group range in between 4 May 2001 and 2 June 2001. Then, the results will be compared with a propagation model and the real swept frequency backscatter ionograms.

### 4.3.1 An Example of a Propagation Model

Figure 4-5 shows the plot of apparent range versus frequency for single hop propagation in a model ionosphere [31]. As stated in section 2.2.2, this propagation has been modeled using the QPS ionospheric model with the methods recommended by the CCIR. The results shown in Figure 4-5 were obtained using an ionospheric model in which foF2 was 9.8 MHz [22]. Details of the simulation are given in [50] and [18].

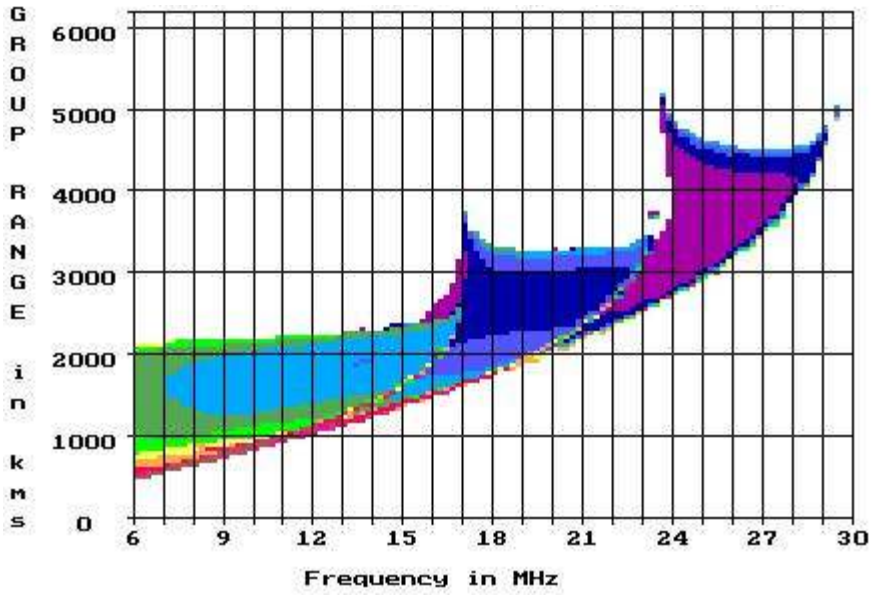


Figure 4-5 Simulated Backscatter Ionogram

The color differences in Figure 4-5 indicate the power level of the backscatter signal but this is not the scope of this thesis, therefore we do not mention about the echo power.

### 4.3.2 Three Examples of Swept Frequency Backscatter Ionogram

During the initial test phase, Bruny Radar has also been operated in a swept frequency mode [22]. As a result, it is possible to obtain swept frequency backscatter ionograms and thus it provides an overview of propagation conditions. The backscatter ionograms when the ionosphere is relatively undisturbed and disturbed are shown in Figure 4-6 and Figure 4-7 respectively [31].

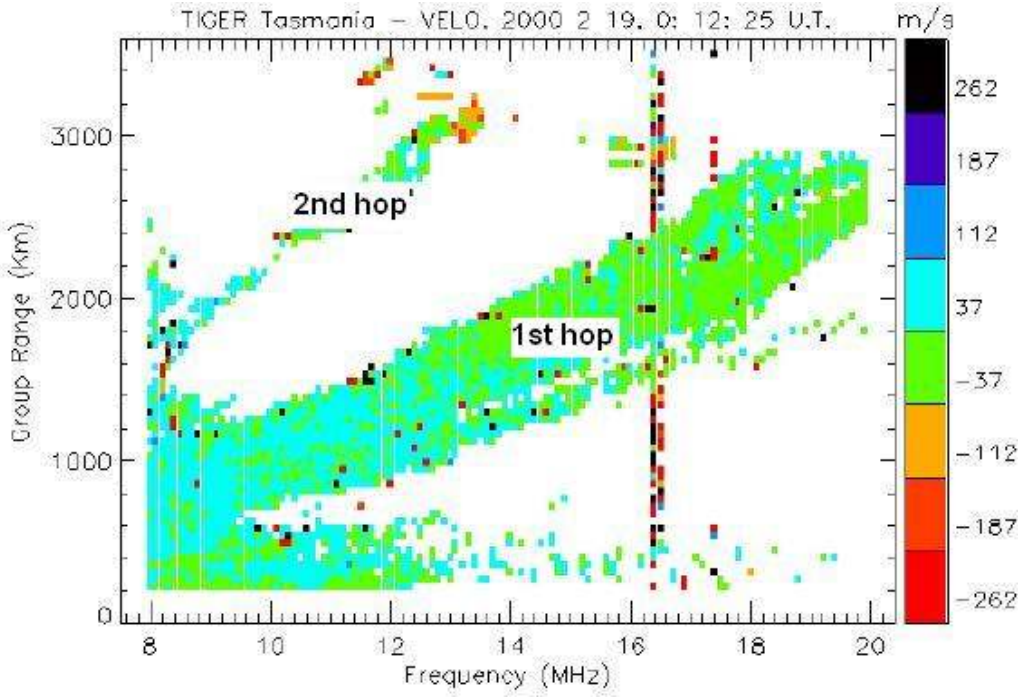


Figure 4-6 Bruny Radar Backscatter Ionogram for the Undisturbed Ionosphere on 19 February 2000, 12:25 UT

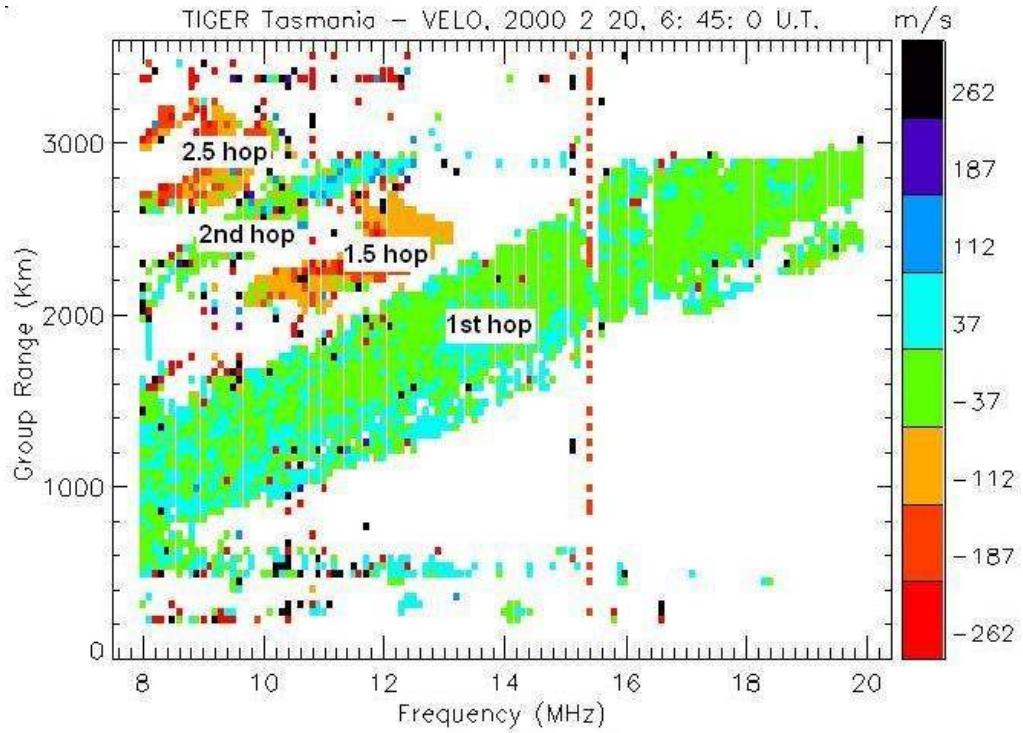


Figure 4-7 Bruny Radar Backscatter Ionogram for the Disturbed Ionosphere on 20 February 2000, 6:45 UT

Figure 4-6 and Figure 4-7 show that the backscatters from ionosphere (1.5 and 2,5 hops) and Earth surface (1 and 2 hops) can be easily differentiated from each other with respect to signatures of the LOS Doppler Velocities.

But there are some cases that the backscatters from ionosphere and Earth surface can not be easily differentiated from each other. Figure 4-8 illustrates that when irregularities are widespread throughout the ionosphere, frequency-range signature of the ionospheric scatter at 1.5 hops is essentially identical to the signature of the one-hop sea scatter [38].

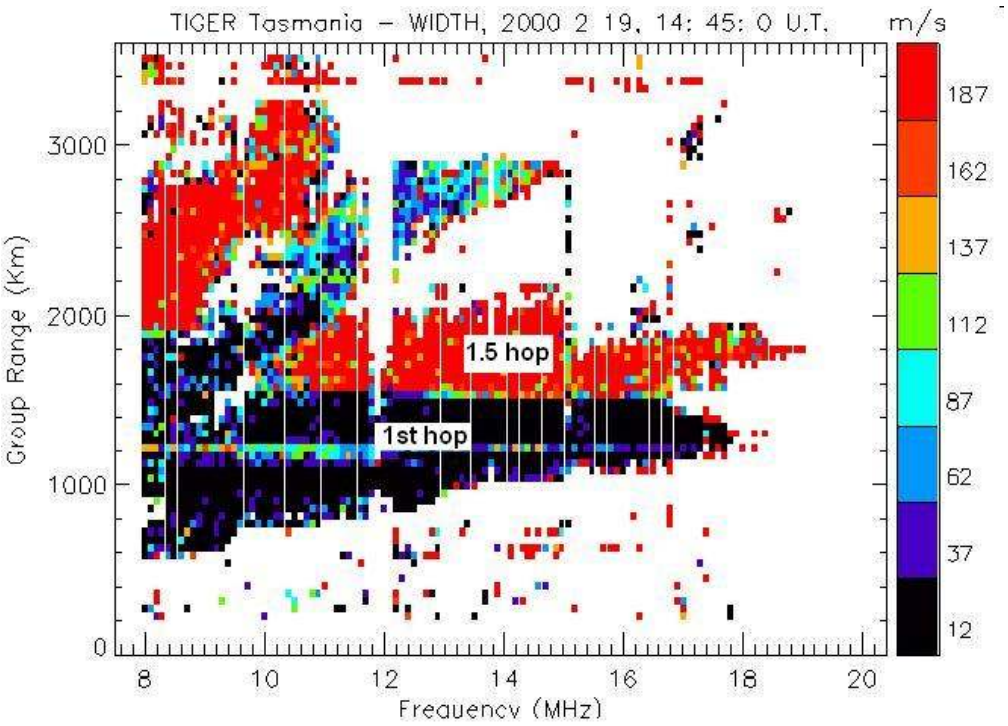


Figure 4-8 Bruny Radar Backscatter Ionogram for the Disturbed Ionosphere on 19 February 2000, 14:45 UT

### 4.3.3 Localization of Ionospheric Backscatters from Summary Plots

If the summary plots for the Bruny Radar [40] are considered in between 4 May 2001 and 2 June 2001, it can be realized that the most of the ionospheric backscatters with LOS Doppler velocities > (+190) m/s and < (-190) m/s are the 1.5 hop scatters.

Sometimes, the signature of the ionospheric backscatters can be differentiated from the ground scatter as in the case of the backscatter shown with the label “2nd 1.5 hop” in Figure 4-9. But sometimes it is not possible to differentiate the ionospheric backscatters from the ground scatter with respect to signatures in the plots. Two examples of this case are shown with the labels “1st 1.5 hop” in Figure 4-9 and “1.5 hop” in Figure 4-10.

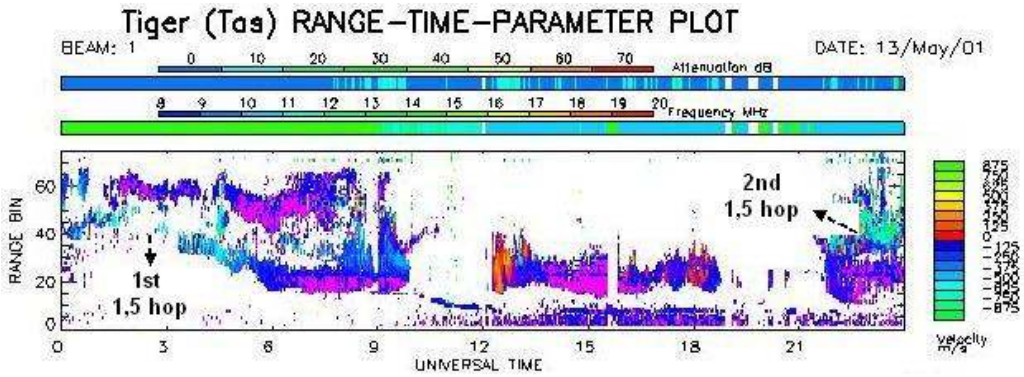


Figure 4-9 Bruny Radar Echo Velocity Plot on 13 May 2001 with 1.5 Hop Scatters

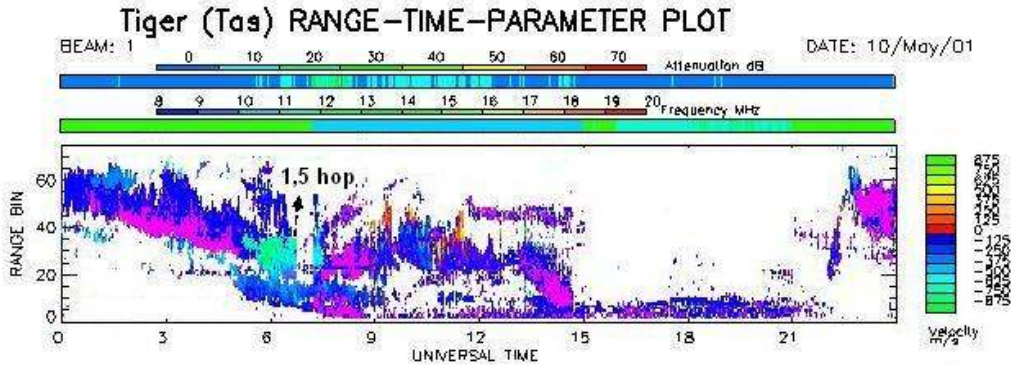


Figure 4-10 Bruny Radar Echo Velocity Plot on 10 May 2001 with 1.5 Hop Scatter

Another important constraint for the localization of the ionospheric backscatters is the operating frequencies of the Bruny Radar. The operating frequencies of the radar are shown with the color bar at the top of the summary plots with the label "Frequency MHz". This is illustrated in Figure 4-11 in detail.

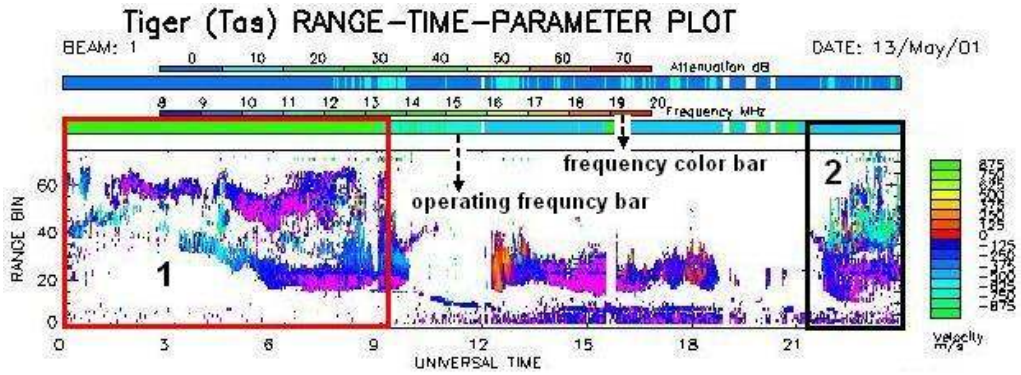


Figure 4-11 Bruny Radar Echo Velocity Plot on 13 May 2001 with Frequencies

The red window frame (also shown with label "1") in Figure 4-11 illustrates that the radar is operating at frequency of ~14 MHz. On the other hand, the black window frame (also shown with label "2") illustrates that the radar is operating at frequency of ~11 MHz.

If the summary plots for the Bruny Radar are considered in between 4 May 2001 and 2 June 2001, it can be realized that the radar is operating mostly at these two frequencies.

As a result, before applying the localization technique for the ionospheric backscatters from Bruny Radar summary plots, the operating frequency of the radar and ionospheric disturbance by magnetic activity (ap) must be taken into account.

Group ranges of the ionospheric backscatters with respect to ap index are given for the two main operating frequencies, ~11 MHz and ~14 MHz, of the Bruny radar in between 04 May 2001 and 02 June 2001 in Table 4-3 and Table 4-4 respectively. Note that the ap index is grouped with two levels of magnetic activity; ap $\leq$ 9 and ap > 9. Former level will be used for undisturbed ionosphere and the letter will be used for disturbed ionosphere.

In the tables, location means the group range of the ionospheric backscatters. Date is in the format of MMDD.

Table 4-3 1.5 Hop Backscatter Group Ranges for the Radar Signal at ~11 MHz.

| **~11 MHz, 1.5 hop** | | |
|---|---|---|
| **ap ≤ 9** | **Group range** | **date** |
| | 1635-2900 | 0511 |
| | 1950-3575 | 0506 |
| **ap > 9** | **location** | **date** |
| | 1950-2900 | 0512 |
| | 1500-2900 | 0513 |
| | 1950-3350 | 0514 |
| | 1950-3800 | 0528 |
| | 2150-3600 | 0602 |
| | 960-2000 | 0515 |
| | 1050-2000 | 0528 |
| | 2150-2700 | 0602 |
| | 1050-3575 | 0516 |
| | 1650-2000 | 0602 |
| | 1725-3125 | 0511 |

Table 4-4 1.5 Hop Backscatter Group Ranges for the Radar Signal at ~14 MHz.

| ~14 MHz, 1.5 hop | | |
|---|---|---|
| | **location** | **date** |
| **ap ≤ 9** | 2085-3575 | 0505 |
| | 2400-2900 | 0517 |
| | 2400-3575 | 0524 |
| | 2400-3350 | 0526 |
| | 2850-3800 | 0530 |
| | 2650-3350 | 0527 |
| | **location** | **date** |
| **ap > 9** | 1750-2200 | 0508 |
| | 1050-2000 | 0509 |
| | 1140-3125 | 0513 |
| | 1050-1550 | 0514 |
| | 2400-3350 | 0504 |
| | 1500-2000 | 0509 |
| | 1275-2000 | 0510 |
| | 1050-1550 | 0512 |
| | 1250-1800 | 0513 |
| | 1050-2000 | 0515 |
| | 1750-2200 | 0508 |

### 4.3.4 HF Radar Group Range Calculations

In this section, group ranges of single hop, 1.5 hop backscatters and the skip distances will be given for the simulated backscatter ionogram and swept frequency backscatter ionograms. And also, calculated group ranges of single hop backscatters and the skip distances from the summary plots will be given both for the disturbed and undisturbed ionosphere. Then some comparisons will be made for the purpose of identification of the propagation medium.

#### 4.3.4.1 HF Radar Operating at ~11 MHz;

1) A single hop can occur between the group ranges of;

    I. 950-2100 km if the simulated backscatter ionogram (Figure 4-5) is considered.

    II. 800-1400 km if the Bruny Radar swept frequency backscatter ionogram for the undisturbed ionosphere (Figure 4-6) is considered.

    III. 950-1800 km if the Bruny Radar swept frequency backscatter ionogram for the disturbed ionosphere (Figure 4-7) is considered.

    IV. 750-1500 km if the Bruny Radar swept frequency backscatter ionogram for the widely disturbed ionosphere (Figure 4-8) is considered.

2) 1.5 hop ionospheric backscatter can occur between the group ranges of;

    I. 2000-2400 km if the Bruny Radar swept frequency backscatter ionogram for the disturbed ionosphere (Figure 4-7) is considered.

    II. 1500-2000 km if the Bruny Radar swept frequency backscatter ionogram for the widely disturbed ionosphere (Figure 4-8) is considered.

3) Skip distance is;

    I. 950 km if the simulated backscatter ionogram (Figure 4-5) is considered.

II. 800 km if the Bruny Radar swept frequency backscatter ionogram for the undisturbed ionosphere (Figure 4-6) is considered.

III. 950 km if the Bruny Radar swept frequency backscatter ionogram for the disturbed ionosphere (Figure 4-7) is considered.

IV. 750 km if the Bruny Radar swept frequency backscatter ionogram for the widely disturbed ionosphere (Figure 4-8) is considered.

#### 4.3.4.2 HF Radar Operating at ~14 MHz;

1) A single ionospheric hop can occur between the group ranges of;

I. 1200-2300 km if the simulated backscatter ionogram (Figure 4-5) is considered.

II. 1100-1900 km if the Bruny Radar swept frequency backscatter ionogram for the undisturbed ionosphere (Figure 4-6) is considered.

III. 1400-2300 km if the Bruny Radar swept frequency backscatter ionogram for the disturbed ionosphere (Figure 4-7) is considered.

IV. 950-1450 km if the Bruny Radar swept frequency backscatter ionogram for the widely disturbed ionosphere (Figure 4-8) is considered.

2) 1.5 hop ionospheric backscatter can occur between the group ranges of;

I. 1450-2000 km if the Bruny Radar swept frequency backscatter ionogram for the widely disturbed ionosphere (Figure 4-8) is considered.

3) Skip distance is;

I. 1200 km if the simulated backscatter ionogram (Figure 4-5) is considered.

II. 1100 km if the Bruny Radar swept frequency backscatter ionogram for the undisturbed ionosphere (Figure 4-6) is considered.

III. 1400 km if the Bruny Radar swept frequency backscatter ionogram for the disturbed ionosphere (Figure 4-7) is considered.

IV. 950 km if the Bruny Radar swept frequency backscatter ionogram for the widely disturbed ionosphere (Figure 4-8) is considered.

#### 4.3.4.3 Bruny Radar Summary Plots

If Table 4-3 is considered, when ap $\leq$ 9, it is realized that 1.5 hop ionospheric backscatter observed is between the group ranges of 1635-2900 km. On the other hand, when ap > 9, it is realized that 1.5 hop ionospheric backscatter is observed between the group ranges of 960-3800 km.

If Table 4-4 is considered, when ap $\leq$ 9, it is realized that 1.5 hop ionospheric backscatter is observed between the group ranges of 2085-3800 km. On the other hand, when ap > 9, it is realized that 1.5 hop ionospheric backscatter is observed between the group ranges of 1050-3350 km.

As stated in section 3.1.2 with Figure 3-2, Since at high latitudes the Earth's magnetic field lines are almost vertical, 1.5 hop ionospheric scatter echoes are detected by HF radars at ranges approximately equal to 1.5 times the range of backscattered ground or sea single hop echoes. Therefore group range of the single hop echo is calculated by the equation 4-3.

$$\text{Single hop group range} = \frac{1.5 \text{ hop group range}}{1.5} \tag{4.3}$$

As a result,

1) When the ionosphere is undisturbed (ap ≤ 9) possible single hop region calculated from the Bruny Radar summary plots is between the group ranges of;

   I. 1090-1950 km for 11 MHz Radar frequency

   II. 1390-2550 km for 14 MHz Radar frequency

2) When the ionosphere is disturbed (ap > 9) possible single hop region calculated from the Bruny Radar summary plots is between the group ranges of

   I. 640-2550 km for 11 MHz Radar frequency

   II. 700-2250 km for 14 MHz Radar frequency

#### 4.3.4.4 Identification of the Propagation Medium

Table 4-5 summarizes the group ranges of single ionospheric backscatters of four different ionograms and the group ranges obtained from the Bruny Radar summary plots. Group ranges are given in km.

Table 4-5 Summary of Possible Single Hop Backscatter Group Ranges in Km.

| | Simulated Backscatter Ionogram | Undisturbed Swept Frequency Ionogram | Disturbed Swept Frequency Ionogram | Widely Disturbed Swept Frequency Ionogram | Summary Plots |
|---|---|---|---|---|---|
| 11 MHz | 950-2100 | 800-1400 | 950-1800 | 750-1500 | ap ≤ 9<br>1090-1950 |
| | | | | | ap > 9<br>640-2550 |
| 14 MHz | 1200-2300 | 1100-1900 | 1400-2300 | 950-1450 | ap ≤ 9<br>1390-2550 |
| | | | | | ap > 9<br>700-2250 |

The group ranges calculated from the Bruny Radar summary plots seem to be around the ones in the ionograms.

If the group ranges calculated from the summary plots are considered, it is very important to note that, when the ionosphere is undisturbed (i.e, ap≤ 9), it is not possible to communicate with a station located within the group range closer than 1090 km for the frequencies 11 to 14 MHz. When the ionosphere is disturbed, skip distance is decreased significantly but it is still not possible to communicate with a station located within the group range closer than 640 km.

Please also note that the terminology of “disturbed” and “undisturbed” ionosphere used in the swept frequency backscatter ionograms and in the summary plots are somewhat different. Many mechanisms and disturbances may produce some degree of backscatter in HF sky wave radar but in this thesis effects of the ionospheric disturbances, which results in small-scale irregularities, with respect to ap index are focused at.

## 4.4 Conclusion

The backscattering of radio waves is a useful form of propagation for the HF frequencies. When the backscatter occurs, it makes the communication possible into the nominal blind zones at unusually high frequencies [13].

In this thesis, it is shown that during the geomagnetic activity measured by the ap index, possibility for the HF signal to backscatter from ionosphere is increased and it is possible to communicate into the nominal blind zones. It also means that, by considering the location of the Bruny Radar, as ap index is increased, intensity of the high latitude F region FAI is increased and these irregularities move to the sub-auroral region as observed by the decreasing group path of the radar beam. Thus, with the increasing magnetic activity and as a result, disturbance state of the ionosphere, possibility for the HF signal to backscatter from ionosphere is increased. In addition to this, the situation of increasing magnetic activity measured by the ap index allows communication into the nominal blind zones.

# CHAPTER 5

# SOME SUGGESTIONS FOR HF RADAR PLANNING AND OPERATION UNDER SPACE WEATHER CONDITIONS

## 5.1 Introduction

In Chapter-4, we studied the relation between the geomagnetic activity measured by the ap index and ionospheric backscatter observance by using a high latitude HF radar summary plots.

Determining the group ranges of the possible ionospheric backscatter echoes and as well as group ranges of single hop backscatter echoes are essential for HF radar planning and operation.

In this chapter, to determine the possible backscatter group ranges in the scope of this thesis, the differences between the high latitude, mid-latitude and low latitude ionosphere, ap forecasting overview and the seasonal and solar cycle variations of Kp will be given by considering the HF radar applications; and than some suggestions for HF radar planning and operation will be given.

## 5.2 High Latitude, Mid-Latitude and Low Latitude Ionosphere

Estimating the possible single hop group range from the 1.5 hop ionospheric backscatter group range is dependent on the FAIs. At the high latitude ionosphere, the Earth's magnetic field lines are almost vertical, therefore group range of the 1.5 hop ionospheric backscatter is approximately equal to 1.5 times the group range of single hop backscatter [22]. On the other hand, the Earth's magnetic field lines at mid-latitudes and low latitudes are not vertical, but rather inclined to the horizontal direction, therefore the receiving conditions of the ionospheric backscatters are

different [20]. Thus, for estimating the single hop group range from the 1.5 hop ionospheric backscatter group range, using effective modeling of the ionosphere together with accurate ray tracing algorithms is very important.

## 5.3 Forecasting the ap Index and the ap Index Variations

### 5.3.1 ap Forecast

As technology advances, the importance of space weather prediction is increasing. Kp is one of the most common indices used to measure the severity of the global magnetic disturbances in Near-Earth space [51]. Since the ap index is nothing but the linear scale converted version of the Kp index, forecasting the Kp and as well as ap indices plays an important role in the prediction of space weather.

There exist some models and organizations estimating ap values. For example [52] supply the estimated values through internet and [51] gives three old and three new examples of the Kp and ap forecast models. Usual inputs for these models are the nowcast Kp, velocity ($V_x$) and density (n) of the solar wind (SW) and the north-south solar magnetospheric component ($B_z$) of the interplanetary magnetic field. The solar wind data can be obtained from the Advanced Composition Explorer (ACE) spacecraft, located upstream at Lagrangian point (L1) [53].

Since the ap index plays an important role for the scope of this study, using the ap forecast models and/or predicted ap index values of the ap forecast organizations, one can obtain possible single hop group ranges and skip distance for the high latitude HF radar application.

### 5.3.2 Solar Cycle Variation

Effects of the solar cycle in the Kp index was investigated in [54]. In that study 27-day averages of the IMF and SW values and Kp index are used from November 1963 through November 1999 and it is showed that there is a solar cycle variation

in the Kp index. Within the data set, there are four solar cycles (20, 21, 22 and 23). The plot on the top in Figure 5-1 shows the variation of the sun spot number R versus time and the bottom plot shows the Kp index versus time [54].

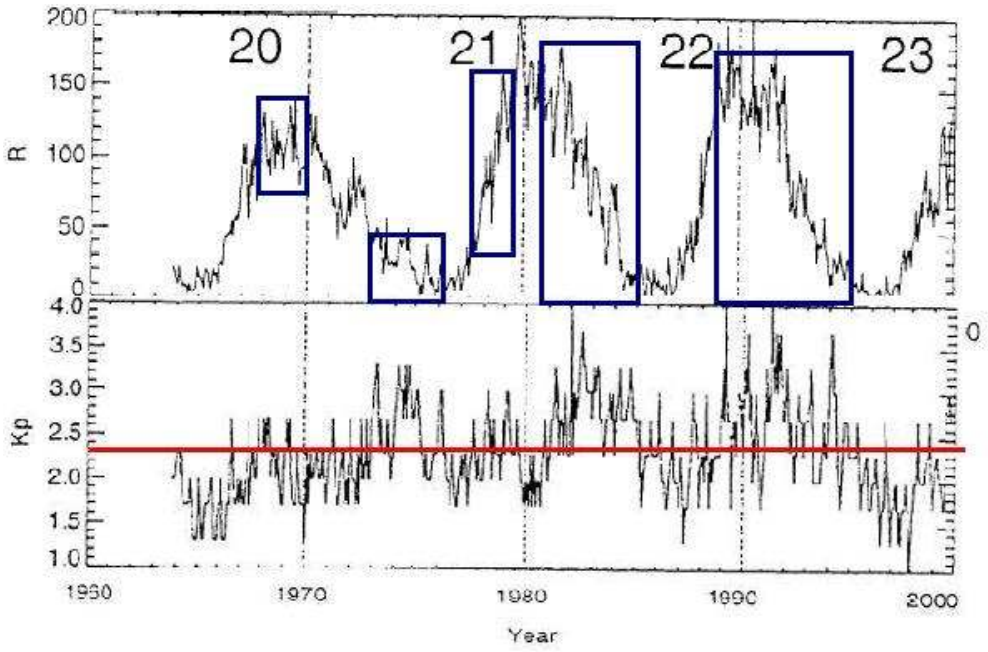


Figure 5-1 Sun Spot Number and Kp Iindex in Solar Cycles 20, 21, 22 and 23

For the scope of this study, Kp values greater than 2+ (i.e., ap=9) are important, therefore the red line in the Kp plot is the Kp values of 2+ and the rectangles with blue frame in the sun spot plot indicates the sun spot values when Kp > 2+. Visual inspection reveals that Kp is greater especially in the declining phase of the solar cycle near solar minimum. In the ascending phase near solar maximum, Kps are still greater than 2+ but less than the Kps of the declining phase of the solar cycle near solar minimum.

As a result it is more probable to observe high latitude F region backscatter in the HF radar beam during the declining phase of the solar cycle near solar minimum. But there is also possible to observe high latitude F region backscatter in the HF radar beam during the ascending phase near solar maximum. We can conclude that the blind zone is smaller in the ascending and declining phases of the solar cycle near solar maximum and minimum respectively.

The correlation is high (i.e., r = 0.82) between the Kp index and the product of the velocity of the SW ($V_{sw}$) and the total IMF ($B_T$), which reveals that total interplanetary electric field ($E_{IMF}$) plays very important role in driving global geomagnetic activity measured by Kp [54]. Equation 5-1 shows this product and Figure 5-2 shows the plot of the product in solar cycles 20, 21, 22 and 23 [54].

$$E_{IMF} = Vsw \times B_T \tag{5- 1}$$

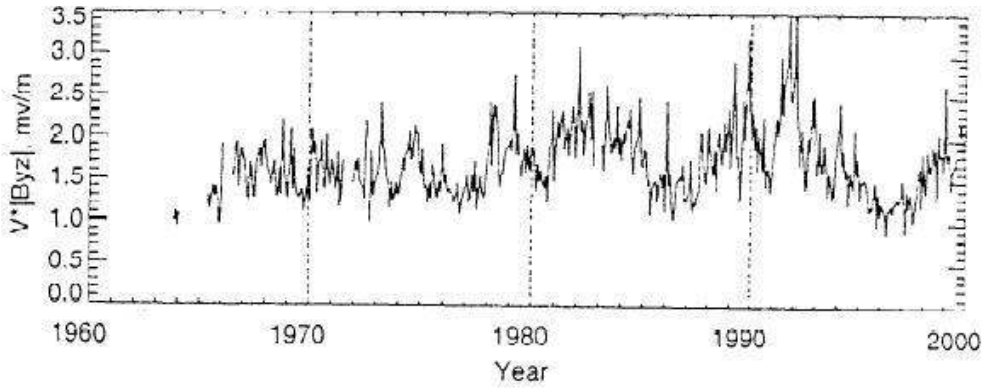


Figure 5-2 $E_{IMF}$ in Solar Cycles 20, 21, 22 and 23

### 5.3.3 Seasonal Variation

The seasonal variation of the Kp index covering the period 1932 to 1995 was investigated in [55]. Data set was restricted to the three Lloyd's seasons, corresponding to Northern Hemisphere summer (May to August), equinox (March, April, September and October) and winter (November to February) and to consecutive occurrence over 6 or 8 three-hourly intervals. Kp was grouped into three parts; Kp values between 0-1 were for quiet times, 2-3 were for transition times and 4-9 were for disturbed times [55].

The seasonal variation of the Kp values between 4-9 with respect to Monthly occurrence frequencies was shown as in Figure 5-3 [55]. In the figure, *Win* stands for winter, *Sum* stands for summer, *equi* stands for equinox and *(6)* and *(8)* stand for consecutive occurrence over 6 or 8 three-hourly intervals respectively.

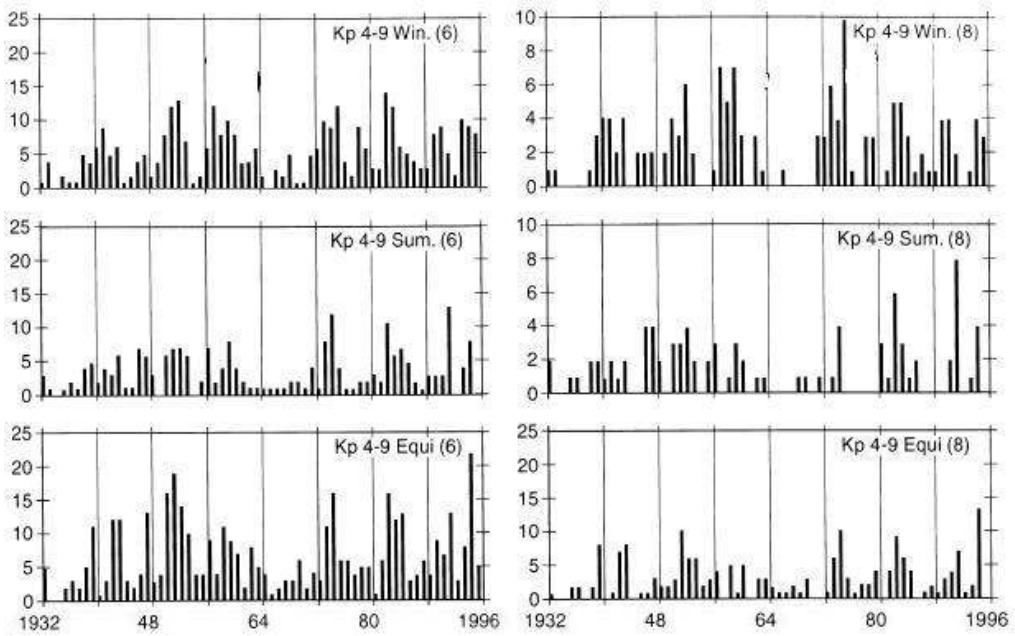


Figure 5-3 Seasonal Occurrence Frequencies of Kp > 4-

From the Figure 5-3, we can conclude that Kp index is greater during equinox and winter than during summer. Thus it is more probable to observe high latitude F region backscatter in the HF radar beam during equinox and winter.

### 5.4 Some Suggestions

In Table 5-1, only the possible group ranges of the single hop propagation are given. Note that these values are taken from Table 4-5.

Table 5-1 Single Hop Group Ranges Calculated from Summary Plots

| Frequency (MHz) | Group Ranges Calculated From Summary Plots (Km) | |
|---|---|---|
| | **ap ≤ 9** | **ap > 9** |
| 11 | 1090-1950 | 640-2550 |
| 14 | 1390-2550 | 700-2250 |

Considering the Table 5-1 and solar cycle and seasonal variation of the ap index, it is possible to give some suggestions to HF radar planner and HF communication planner for the radar operating at the frequencies 11MHz and 14 MHz:

I. Since it is more probable to observe ap index greater than 9 during the declining phase of the solar cycle near solar minimum and during the ascending phase near solar maximum, it is not possible to communicate with the station located within the group range of 640 km at 11MHz and 14 MHz.

II. But in the other phases of the solar cycle, since it is more probable to observe ap index smaller than 9, it seems that it is not possible to communicate with the station located within the group range of 1950 km at 11MHz and 2550 km at 14 MHz.

III. Since it is more probable to observe ap index greater than 9 during equinox and winter, it is not possible to communicate with the station located within the group range of 640 km at 11MHz and 14 MHz.

IV. But in the summer, since it is more probable to observe ap index smaller than 9, it seems that it is not possible to communicate with the station located within the group range of 1950 km at 11MHz and 2550 km at 14 MHz.

V. It seems that the maximum group range of the HF signal for the single hop propagation does not change significantly with respect to the operating frequencies for 11 MHz and 14 MHz. Therefore there is no constraint about the maximum group ranges for the given frequencies. Actually HF signal can propagate to group ranges of up to 4000 km via second hops.

Situation given in I and III is shown in Figure 5-4 and situation given in II and IV is shown in Figure 5-5 with the radar operates at 11 MHz.

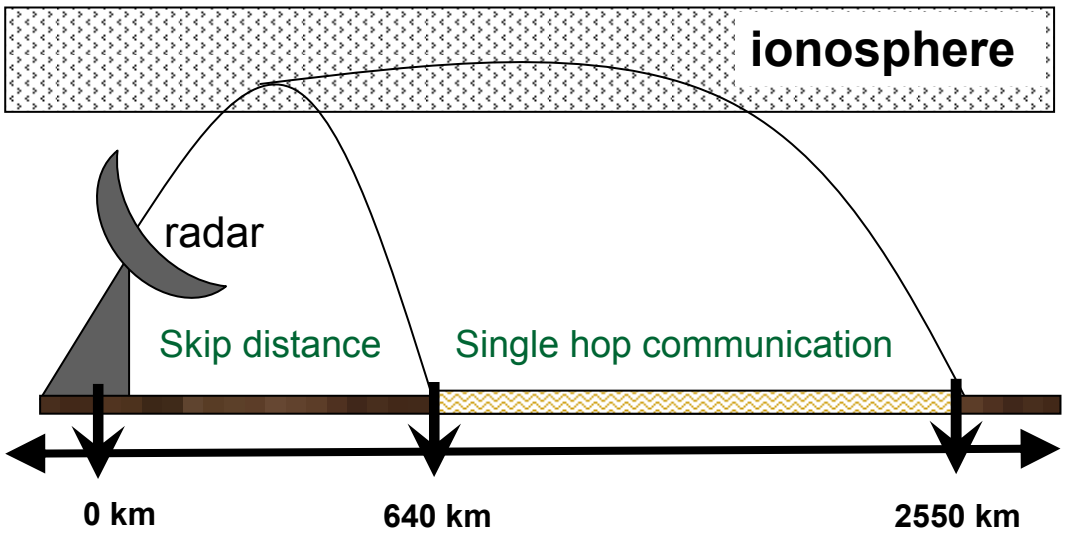


Figure 5-4 Possible Skip Distance when ap > 9

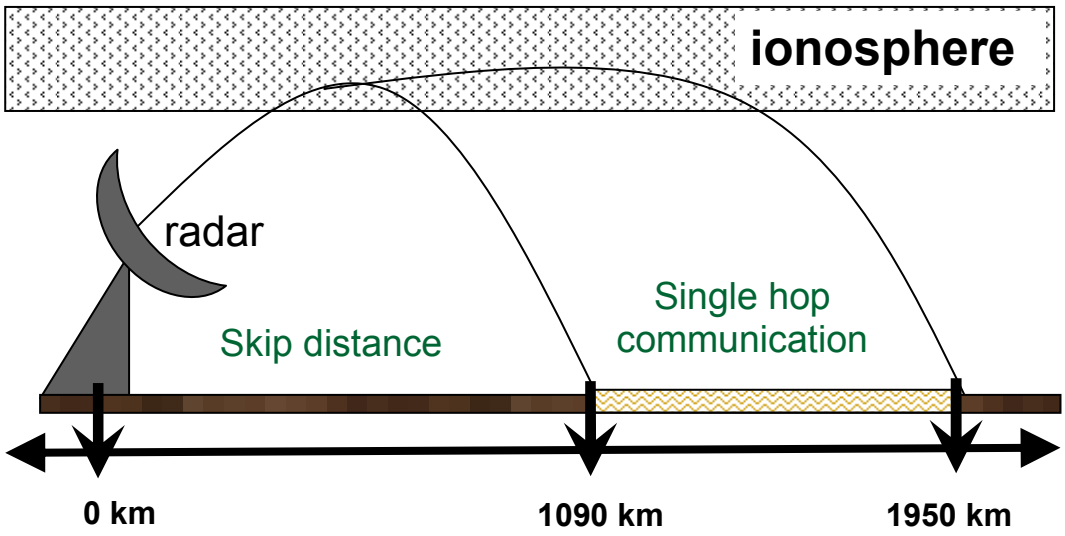


Figure 5-5 Possible Skip Distance when ap ≤ 9

ap forecasting models and organizations make it possible to forecast the ap index one to four hours ahead, therefore it is possible for the HF radar operator and HF

communication operator to estimate the possible skip distance and possible single hop group ranges for the given frequencies of 11 MHz and 14 MHz.

The method used in this thesis is general, therefore if a campaign having raw data is done, it is possible to obtain more precise results.

# CHAPTER 6

# CONCLUSIONS AND FUTURE STUDIES

## 6.1 Summary and Conclusions

In this thesis, the use of HF radar system is considered from the identification of the ionospheric propagation medium point of view.

HF radar system has been identified globally under ionospheric disturbances and some operational suggestions have been presented. Doppler velocity is considered as the characteristic parameter of the propagation medium and dependence of Doppler velocity and group range of the echo signal on ap index is examined.

In the beginning of the thesis, considering the Doppler velocity of the HF radar echoes, backscatter observance data from the high latitude F region of the ionosphere are generated semi-synthetically from the TIGER HF Radar experiment over the dates between 29 March 2001 and 26 February 2002. ap index of the same interval is obtained from National Geophysical Data Center's database [49].

Secondly, the dependency of the ionospheric backscatter observance on the ap index is presented.

Thirdly, over the dates between 4 May 2001 and 2 June 2001, considering again the Doppler velocity of the HF radar echoes, for 11MHz and 14 MHz radar frequencies, group ranges of the backscatter signals from the high latitude F region of the ionosphere are generated semi-synthetically and the dependency of the group ranges on the ap index is presented. After that, possible group ranges and blind zones under ionospheric disturbance measured by the ap index for the single hop propagation at the given frequencies are presented.

Finally, considering the differences between the high latitude and mid-latitude ionosphere, ap prediction methods and the seasonal and solar cycle variations of Kp and ap indices, some suggestions for the HF radar planning and operation are given.

This approach considers the HF radar as a system and identifies the system by considering communication system planning and operation under ionospheric disturbances.

In this thesis, only ap index is used, but it is easy to use other global magnetic indices such as Dst and AE and local indices such as PC. If any local index is to be used then the correct local value should be selected and the local parameter should characterize the backscatter region of the selected HF radar.

The method used in this thesis is general, therefore the given suggestions can be used for industrial or other types of systems with similar characteristics. HF radar system is considered in this thesis as an interesting and involved example. Since Space Weather is a new concept which is attracting a great deal of attention in the international scientific and technological circles [56], the approach is also interesting in the sense that it deals with the effects of space weather on communication.

### 6.2 Future Work

Since the Local Magnetic Time (MLT) is the appropriate local time reference for many space weather phenomena [31], identification of the medium can also be done with respect to the MLT.

Two or more relevant indices can be included and the improvements can be examined. The effects of included local magnetic indices can also be investigated.

With the data having higher resolution or with the raw data of the same experiment, the thesis can be repeated for the E-layer-only backscatters and sea-only

backscatters to identify the propagation paths of the location in which the experiment is held.

The thesis can be extended to longer duration data to increase the sensitivity of the statistical analysis.

## REFERENCES

[1] Reza Dizaji, “HFSWR, A Radar Technology to See Beyond Horizon Signal Processing Challenges”, IEEE Toronto Section, IEEE Toronto Signals and Applications Chapter, November 2004.

[2] Merrill I. Skolnik, Radar Handbook, Second Edition, McGraw-Hill Publishing Company, International Edition, 1991, pages 24.1-24.40, HF Over-The-Horizon Radar.

[3] Keisuke Hosokowa, Toshihiko Iyemori, Akira Sessai Yukimatu, Natsuo Sato, “Source of field-aligned irregularities in the subauroral F region as observed by the SuperDARN radars”, Journal of Geophysical Research, Vol.106, no. A11, pages 24,713-24,731, November 1, 2001.

[4] R. A. Makarevitch, F. Honary and A. V. Koustov, “Simultaneous HF measurements of E- and F-region Doppler velocities at large flow angles”, Annales Geophysicae (2004) 22: 1177–1185 SRef-ID: 1432-0576/ag/2004-22-1177, European Geosciences Union 2004, 2 April 2004.

[5] J. A. Ratcliffe, An Introduction to the Ionosphere and Magnetosphere, Cambridge University Press, 1972, pages 37-99, The ionospheric layers. The sub-peak ionosphere.

[6] Sandro M. Radicella Head, “The Quiet and Disturbed Ionosphere First Lecture”, Aeronomy and Radiopropagation Laboratory, The Abdus Salam International Centre for Theoretical Physics (ICTP), 2004.

[7] Alfread J. Bogush, Jr., Radar and the Atmosphere, DESE Research and Engieering, Inc., 1989, pages 251-252, The Thermosphere.

[8] Adolph S. Jursa (Scientific Editor), Handbook of Geophysics and the Space Environment, Air Force Geophysics Laboratory, Air Force Systems Command, United State Air Force, pages 9-1, 9-2, Ionospheric Layers, pages 10-28, VLF/LF Propagation, pages 10-36, MF Propagation, Document Accession Number: ADA 167000, 1985.

[9] R.D. Hunsucker, J.K. Hargreaves, The High-Latitude Ionosphere and Its Effects on Radio Propagation, Cambridge University Press, pages23-48, The Main Ionospheric Layers, 2003.

[10] Sandro M. Radicella Head, "The Quiet and Disturbed Ionosphere Second Lecture", Aeronomy and Radiopropagation Laboratory, The Abdus Salam International Centre for Theoretical Physics (ICTP), 2004.

[11] "A New Approach For The Assessment of HF Channel Availability Under Ionospheric Disturbances", A Thesis Submitted to the Graduate School of Natural and Applied Sciences of the Middle East Technical University by Murat Özgür Sarı, September 2006.

[12] "Radio Communications in the Digital Age", Harris Corporation, RF Communications Division Radio Communications in the Digital Age, Volume One: HF Technology, Edition 2, Library of Congress Catalog Card Number: 96-94476, October 2005.

[13] Edwin C. Jones, Harold C. Diezel, Raymond A. Greenwald, Hans-Peter Helfert, "HF Backscatter off Traveling Ionospheric Disturbances Identified with Pactor-II", http://ecjones.org/backscatter.html, 7 September 2006.

[14] R. J. Norman, M. L. Parkinson, and P. L. Dyson, "Mapping the Ionosphere Using a HF Radar Backscatter Inversion Technique", Proceedings of the sixth Workshop on the Applications of Radio Science, Leura, Australia, February 2006.

[15] T. W. Bennington, Short-Wave Radio and the Ionosphere, Second Edition, Engineering Division, British Broadcasting Corporation, Iliffe & Sons, LTD., 1950, page 80.

[16] The National Oceanic and Atmospheric Administration (NOAA) Space Environment Center, http://www.sec.noaa.gov/, May 2006

[17] D. Bilitza, "International Reference Ionosphere 2000", Radio Science, Volume 36, Number 2, pages 261-275, 2001.

[18] P.L. Dyson, J.A. Bennett, BE, "Exact ray path calculations using realistic ionospheres", IEE Proceedings-H, vol. 139, pp. 407-413, 1992.

[19] High Frequency Propagation Models, Institute of Telecommunication and Sciences, http://elbert.its.bldrdoc.gov/hf.html, February 1997.

[20] Nozomu Nishitani and Tadahiko Ogawa, "Model calculations of possible ionospheric backscatter echo area for a mid-latitude HF radar", Adv. Polar Upper Atmos. Res., 19, 55-62, 2005, 2005 National Institute of Polar Research, 5 April 2005.

[21] R. Michael Jones, Judith J. Stephenson, "A versatile three-dimensional ray tracing computer program for radio waves in the ionosphere", U.S. Department of Commerce, OT Report 75-76, 1975

[22] Peter L. Dyson, Robert J. Norman and Murray L. Parkinson, "Ionospheric Propagation Modes Identified Using the TIGER HF Radar", Proceedings of the Workshop on the Applications of Radio Science, Leura, Australia, February 2002.

[23] Second CCIR computer-based interim method for estimating sky-wave field strength and transmission loss at frequencies between 2 and 30 MHz, CCIR, 1978.

[24] Tulunay E., Senalp E.T., Cander Lj. R., Tulunay Y., Bilge A.H., Mizrahi E., Kouris S.S., Jakowski N., "Development of algorithms and software for forecasting, nowcasting and variability of TEC", Annals of Geophysics, 47(2/3), pp. 1201-1214, 2004.

[25] Tulunay Y., Tulunay E., Senalp E.T., "The Neural Network Technique-1: A General Exposition", Adv. Space Res.,33(6), pp. 983-987, 2004-a.

[26] "Monitoring the Near-Earth Space Environment", Earth Observation Magazine (EOM), Volume 4, Issue 2, February 2005.

[27] N. B. Crosby, M. J. Rycroft and Y. Tulunay, "Overview of a Graduate Course Delivered in Turkey, Emphasizing Solar-Terrestrial Physics and Space Weather, Surveys in Geophysics", (2006) 27, DOI: 10.1007/s10712-005-6204-3, 2006, pages 319-364.

[28] M. Musa and S. Salous, "Ambiguity Elimination in HF FMCW Radar Systems", IEE Proceedings-Radar, Sonar and Navigation, vol.147, No. 4, pp 182-188, August 2000.

[29] Philippe Lacomme, Jean- Philippe Hardange, Jean-Claude Marchais, Eric Normant, Air and Spaceborn Radar Systems, An Introduction, William Andrew Publishing, LLC, 2001, pages 1-2.

[30] D.H. Sinnott, "The Development of Over-the-Horizon Radar in Australia", DSTO Bicentennial History Series, ISBN 0 642 13561 4, 1988.

[31] Peter L. Dyson and John C. Devlin, "The TIGER Radar - An Extension of SuperDARN to sub-auroral latitudes", WARS'00 (Workshop on Applications of Radio Science) Proceedings, pp. 9-31, 2000.

[32] J.C. Cerisier, J.P. Villain, Séran, A. Marchaudon, “Plasma convection in the magnetosphere and the SuperDARN network”, Meeting of the Société française d'Astronomie et d'Astrophysique, 24-29 June 2002

[33] J. C. Foster and H. B. Vo, “Average Characteristics and Activity Dependence of the Subauroral Polarization Stream”, MIT Haystack Observatory, Westford, MA, Journal of Geophysical Research (Space Physics), Volume 107, Issue A12, pp. SIA 16-1, Cite ID 1475, 2002.

[34] An International Radar Network for Studying the Earth's Upper Atmosphere, Ionosphere, and Connection into Space, Super Dual Auroral Radar Network (SuperDARN), http://superdarn.jhuapl.edu/, January 2007.

[35] R. A. Greenwald, K. B. Baker, J. R. Dudeney, M. Pinnock, T. B. Jones, E. C. Thomas, J. P. Villain, J. C. Cerisier, C. Senior, C. Hanuise, R. D. Hunsucker, G. Sofko, J. Koehler, E. Nielsen, R. Pellinen, A. D. Walker, N. Sato, and H Yamagishi, “DARN/SuperDARN - a global view of the dynamics of high-latitude convection”, Space Science Reviews, 71:761-796, 1995.

[36] Tasman International Geospace Environmant Radars, La Trobe University, http://www.tiger.latrobe.edu.au/, March 2005.

[37] R. J. Norman, M. L. Parkinson and P.L. Dyson, “Comparing HF Radar Backscatter from the Southern Ocean with Ray-Tracing Results Using The IRI Model”, Proceedings of the Fifth Workshop on the Applications of Radio Science, 2004.

[38] Murray L. Parkinson, John C. Devlin, Peter L. Dyson, J. S. Whittington, “The Tasman International Geospace Environment Radar (TIGER) Current Development and Future Plans”, Proceedings of the International Conference on, 3-5 September 2003, pp. 363-367.

[39] Longsong HE, Peter DYSON, Murray L. PARKINSON, Phillip J. WILKINSON, and Weixing WAN, "Medium-Scale Traveling Ionospheric Disturbances Studied with the TIGER HF SuperDARN Radar", Proceedings of the Workshop on the Applications of Radio Science, 2002.

[40] TIGER Summary Data, Centre for Space Physics Research the School of Mathematical and Physical Sciences, The University of Newcastle, http://plasma.newcastle.edu.au/plasma/research/tiger/sdata.htm, August 2006.

[41] Gao Huotao, Li Geyang, Li, Yongxu, Yang Zijie, and Wu Xiongbin, "Ionospheric Effect of HF Surface Wave Over-The-Horizon Radar", Radio Science, Volume 41, Issue 6, CiteID RS6S36, 2006.

[42] Kenneth Davies, Ionospheric Radio, Peter Peregrinus Ltd, 1990, page 187.

[43] C. Hanuise, J. P. Villain, C. Beghin, G. Caudal, "Small Scale Irregularities In The High-Latitude F Region", Advisory Group For Aerospace Research & Development (AGARD) Conference Proceedings No.382, Propagation Effects on Military Systems in the High latitude Region, 1985.

[44] Melissa G. Meyer, John D. Sahr and Andrew Morabito, J, "A Statistical Study of Subauroral E-Region Coherent Backscatter Observed Near 100 MHz With Passive Radar", GR - Space Physics, Vol. 109, A07308, American Geophysical Union, 2004.

[45] K. Hosokawa, M. Sugino, M. Lester, N. Sato, A. S. Yukimatu and T. Iyemori, "Simultaneous Measurement of Duskside Subauroral Irregularities From The CUTLASS Finland Radar and EISCAT UHF system", Journal Of Geophysical Research, Vol. 107, No. A12, 1457, 2002.

[46] M. M. Fares Saba, W. D. Gonzalez, A. L. Clua de Gonzalez, “Relationships between the AE, ap and Dst indices near solar minimum (1974) and at solar maximum (1979)”, Annales Geophysicae 15, 1265-1270, 1997.

[47] Geomagnetic Kp and ap indices, National Geophysical Data Center (NGDC), NOAA Satellite and Information Service, http://www.ngdc.noaa.gov/stp/GEOMAG/kp_ap.html, August 2006.

[48] Linda M. Burke, Bruce A. Toth, Simon P. Wing, Janice M, “Predicting Geomagnetic Activity and Storms, Extended Forecasting Kp Requirements”, UPOS-180-01, Version 1.0, Schofield University Partnering for Operational Support (UPOS), Space Weather Products, July 15, 2005,

[49] National Geophysical Data Center, Geomagnetic Data Online ftp://ftp.ngdc.noaa.gov/STP/GEOMAGNETIC_DATA/INDICES/KP_AP/, August 2006

[50] Dyson, P.L. and Bennett, J.A., “A model of the vertical distribution of the election concentration in the ionosphere and its application to oblique propagation studies”, J. of Atmospheric and Terrestrial Physics, 50, (3), pp. 252-262., 1988.

[51] S. Wing, J. R. Johnson, J. Jen, C.-I. Meng, D. G. Sibeck, K. Bechtold, J. Freeman, K. Costello, M. Balikhin, and K. Takahashi, “Kp Forecast Models”, JOURNAL OF GEOPHYSICAL RESEARCH, VOL. 110, A04203, 2005

[52] CALSPACE Lockhedd/VC Berkeley Center of Excellence, Space Weather, Space Physics Research Group, University of California, Berkeley. http://sprg.ssl.berkeley.edu/htbin/forecast/AuroralKp.pl, December 2006.

[53] Advanced Composition Explorer (ACE), http://www.srl.caltech.edu/ACE/, October 2006.

[54] V. O. Papitashvili, N. E. Papitashvili, J. H. King, “Solar Cycle Effects in Planetary Geomagnetic Activity: Analysis of 36-Year Long OMNI Dataset”, Geophysical Research Letters, Vol.27, No.17, pages 2797-2800, 2000.

[55] G. K. Rangarajan, T. Iyemori, “Time variations of geomagnetic activity indices Kp and Ap: an update”, Ann. Geophysicae 15, 1271-1290, 1997.

[56] Tulunay E., Senalp E.T., Radicella S.M., Tulunay Y., “Forecasting Total Electron Content Maps by Neural Network Technique”, Radio Sci., 41(4), RS4016, 2006.